

# Complete gravity field of an ellipsoidal prism by Gauss–Legendre quadrature

C. Roussel,<sup>1</sup> J. Verdun,<sup>1</sup> J. Cali<sup>1</sup> and F. Masson<sup>2</sup>

<sup>1</sup> Laboratoire Cnam-GeF/GRGS (EA 4630) École Supérieure des Géomètres et Topographes (Cnam/ESGT) 1 boulevard Pythagore, 7200, Le Mans, France.

E-mail: [jerome.verdun@cnam.fr](mailto:jerome.verdun@cnam.fr)

<sup>2</sup> IPGS/EOST, Université de Strasbourg/CNRS, Bâtiment Descartes 5, rue René Descartes, 67084, Strasbourg cedex, France

Accepted 2015 October 7. Received 2015 October 6; in original form 2015 February 20

## SUMMARY

The increasing availability of geophysical models of the Earth's lithosphere and mantle has generated renewed interest in computation of theoretical gravity effects at global and regional scales. At the same time, the increasing availability of gravity gradient anomalies derived from satellite measurements, such as those provided by GOCE satellite, requires mathematical methods that directly model the gravity gradient anomalies in the same reference frame as GOCE gravity gradients. Our main purpose is to interpret these anomalies in terms of source and density distribution. Numerical integration methods for calculating gravity gradient values are generally based on a mass discretization obtained by decomposing the Earth's layers into a finite number of elementary solid bodies. In order to take into account the curvature of the Earth, spherical prisms or 'tesseroids' have been established unequivocally as accurate computation tools for determining the gravitational effects of large-scale structures. The question which then arises from, is whether gravity calculation methods using spherical prisms remain valid when factoring in the ellipticity of the Earth. In the paper, we outline a comprehensive method to numerically compute the complete gravity field with the help of the Gauss–Legendre quadrature involving ellipsoidal shaped prisms. The assessment of this new method is conducted by comparison between the gravity gradient values of simple sources obtained by means of numerical and analytical calculations, respectively. A comparison of the gravity gradients obtained from PREM and LITHO1.0 models using spherical- and ellipsoidal-prism-based methods is also presented. Numerical results indicate that the error on gravity gradients, caused by the use of the spherical prism instead of its ellipsoidal counterpart to describe an ellipsoidally shaped Earth, is useful for a joint analysis with those deduced from GOCE satellite measurements. Provided that a suitable scaling of prism densities has been performed, the spherical approximation error at GOCE height hardly reaches 1 mE for the entire Earth's lithosphere. The error attains 6 mE at a peak for a complete modeling of the Earth, from the crust down to the internal core.

**Key words:** Numerical approximations and analysis; Satellite geodesy; Gravity anomalies and Earth structure; Geopotential theory.

## 1 INTRODUCTION

The current increasing availability of satellite-measured gravity data covering the whole Earth combined with increasingly reliable geophysical models of the Earth's lithosphere and mantle has generated renewed interest in the computation of theoretical gravity effects at global and regional scales from geological models (Arabelos & Tsoulis 2013). The latest gravity satellite mission GOCE has provided data of unprecedented resolution and accuracy at global and regional scales (Yi & Rummel 2013) through the use of a

satellite orbiting at low altitude—260 km, mean altitude in the nominal phase—and equipped with an ultra-sensitive gradiometer for directly measuring the gravity gradients (Rummel *et al.* 2011). Gravity models based solely on satellite data (satellite-only gravity models) provided by GOCE—also combined with other gravity satellites such as GRACE and LAGEOS—are commonly expressed in terms of Stokes' coefficients as a spherical harmonics expansion up to degree and order 280, for example, the TIM R5 gravity model (Brockmann *et al.* 2014), or even degree and order 300, for example, the DIR R5, which methodology is described in Bruinsma

*et al.* (2013). The theoretical spatial resolution of such gravity models is of 70 km (half-wavelength), which is suitable for regional geophysical studies. For more local scales, the spherical harmonics expansions can be significantly extended to higher degrees by including the terrestrial gravity data measured over the Earth's continents and the surface gravity data provided by satellite altimetry. For instance, the maximum spherical harmonic degree attained in the EGM2008 gravity model (Pavlis *et al.* 2008) and the recently presented EIGEN-6C4 gravity model (Förste *et al.* 2014) is of 2190, which corresponds to a theoretical spatial resolution of 9 km.

Moreover, significant improvements in knowledge of the lithosphere have been obtained, particularly through seismology advances. In parallel, accurate global digital elevation models, which include notably satellite-measured land topography and ocean bathymetry deduced from satellite altimetry and depth soundings (Smith & Sandwell 1997), have become available, thus giving a fairly accurate image of the Earth's land surface and sea bottom. Seismological and elevation models combined with other geological and geophysical models, giving for instance sediment thickness or the depth of Mohorovičić's discontinuity (Moho), represent geolocated data for areas ranging in size from a few degrees to global coverage of the entire planet. Hence, such a crustal model as CRUST1.0 (Mooney 1998; Laske *et al.* 2013), based onETOPO1 global relief model (Amante & Eakins 2009), provides the density distribution inside the crust divided into eight separate layers—ice, water, soft, middle and hard sediment, upper, middle and lower crust—from the Earth surface down to the Moho and the density value just beneath the Moho on a  $1^\circ \times 1^\circ$  grid. Quite recently, a new model at  $1^\circ$  resolution named LITHO1.0 (Pasyanos *et al.* 2014) has been developed that offers an extension of crust models down to the asthenosphere by including the lithospheric mantle (lid). The use of CRUST1.0 as an initial model of the Earth's crust in the inversion allows it to be consistent with LITHO1.0. The availability at a time of lithospheric models and the gravity gradients provided by the GOCE satellite at whatever area around the Earth, offers us the unique opportunity to determine regional gravity gradient anomalies for lithospheric interpretation (Bouman *et al.* 2015), and for mapping the density distribution beyond the lithosphere up to the Earth's mantle (Panet *et al.* 2014).

Interpreting gravity gradient anomalies derived from GOCE satellite measurements in terms of source and density distribution requires mathematical methods that directly model the gravity gradients (consisting of the nine second-order derivatives of the gravity potential, also known as Marussi's tensor) due to large scale, arbitrarily shaped sources of variable density. The gravity gradients previously mentioned are actually gravitational gradients, since gravity gradients also include the rotation of the mass source. The Earth's rotation is well known and not considered if we assume that the gravitational gradients produced by the mass source can be interpreted as the differences between the measured gravity gradients and those deduced from an Earth model, also known as gravity gradient anomalies. From this point forward, we will only use the term gravity gradients.

For the purpose of comparison, the gravity gradients obtained by numerical computation have to be expressed in the same local north-oriented frame—denoted by LNOF (Bouman *et al.* 2013)—as those currently available for geophysical applications, derived from GOCE data by scientists specialized in space gravimetry (Gruber *et al.* 2014). The starting point of every numerical method for calculating gravity gradients, relies upon the gravity potential since gravity gradients can be calculated from the gravity potential by applying linear operators. The density distribution, given for instance

by geological models of the Earth, is only available in discrete form, for example, consisting of a regular grid of evenly spaced, geolocated points. Thus, the numerical computation of the gravity potential requires a mass discretization obtained by decomposing the Earth's layers into a finite number of elementary solid bodies. As matters stand, the need to employ spherical prisms or 'tesseroids' to accurately compute the gravity effects of large-scale structures, for which the Earth's curvature must be considered, has been established unequivocally (Heck & Seitz 2007; Wild-Pfeiffer 2008), especially as the computation can be carried out in acceptable computation time (Grombein *et al.* 2013). Furthermore, the algorithms currently used in many programs of geophysical forward modeling are still based on a flat Earth approximation. Such an approximation has proven to be inadequate for computing gravity gradients of Earth's sources comparable to GOCE gravity gradients expressed in the LNOF (Bouman *et al.* 2013). An additional processing is then required to transform the gravity gradients initially computed in the flat model reference frame to the LNOF. It is likely to be more advantageous to directly calculate the gravity gradients in the LNOF.

Numerous approaches have been adopted to numerically evaluate gravity field constituents for a tesseract volume depending on the requirements of the specific applications in the fields of geophysics as well as in physical geodesy. Because there is no analytical formula giving the gravity effects of a tesseract, calculations have to be conducted by means of approximate methods of integral calculus. In their innovative attempt to model the gravity effects of the spherical Earth, Ku (1977) and von Frese *et al.* (1981a) derived a least-squares-based method to determine the distribution of point sources equivalent to the anomalous solid body generating the same gravity anomaly as the one observed. In such a method, the disturbing point sources within the anomalous body and their masses can be estimated according to a Gauss-Legendre quadrature (GLQ) decomposition of the integral involved in the expression giving the anomalous body gravity field. The resulting equivalent point sources can then be used to directly calculate the gravity effects of arbitrary mass distributions (von Frese *et al.* 1981b). More recently, GLQ has been used to numerically estimate the potential of a tesseract and its first and second derivatives (Asgharzadeh *et al.* 2007; Wild-Pfeiffer 2008). Software such as Tesseroids (Uieda *et al.* 2011; Uieda 2013) is a sequel to these two papers, thus allowing the complete gravity field of an arbitrary mass distribution defined in spherical coordinates to be calculated.

Other approaches have also been discussed involving alternative mathematical methods for modeling the spherical prism (Johnson & Litehiser 1972; Cochran & Talwani 1978; Smith *et al.* 2001). For instance, Petrović (1996) and Tsoulis (2012) derived analytical expressions of the gravitational potential and its first and second derivatives for polyhedral bodies using line integrals. Alternatively, some algorithms developed in Tsoulis *et al.* (2009) can directly provide the finite set of Stokes' coefficients involved in the spherical harmonics expansion of the gravity potential of an arbitrarily shaped polyhedral body. The transformation of the gravity anomalies produced by rectangular prisms has been explored by some authors (Talwani & Ewing 1960; Nagy 1966; Paul 1974; Plouff 1976; Ku 1977; Nagy *et al.* 2000), especially with the help of exact analytical formulae for calculating gravity effects of the rectangular prism. The flat top of rectangular prisms can be replaced by a smooth surface to advantageously accommodate more complex mass sources (Tsoulis *et al.* 2003). Some other approaches rely upon a Taylor series expansion of the gravity potential integral kernel in the spirit of MacMillian (1930), who was the first to

develop the theory for the gravity potential of a rectangular prism. Heck & Seitz (2007) utilized a third-order Taylor expansion to evaluate the tesseroid gravity potential and its first radial derivative, which is the radial component of the gravity vector. Wild-Pfeiffer (2008) extended the method to all the second derivatives of the tesseroid gravity potential, thus providing the complete gravity field of a tesseroid (gravity vector and Marussi's tensor) and, recently, Grombein *et al.* (2013) have proposed optimal formulae that differ from the previous in that Cartesian integral kernels are involved instead of spherical ones and that also apply to the Poles, which permit the computation time to be significantly decreased. Finally the semi-analytical method proposed by Heck & Seitz (2007) consists in analytically solving the one-dimensional integral involved in the gravity potential, which depends on the radial distance and numerically evaluating the remaining two-dimensional integral by means of a quadrature.

The question which then arises is whether gravity calculation methods using spherical prisms remain valid for calculating the gravity effects produced by larger structures than those encountered in the topography or the crust and for which the ellipticity of the Earth must be taken into account. Whether such an approximative calculation method is effective cannot be settled in isolation; it makes more sense to ask whether the accuracy of calculated gravity values is adequate for some stated purposes involving newly acquired gravity data. As an illustration, the accuracy of the gravity gradients provided by the GOCE satellite mission within spectral ranges suitable for geological applications is expected to be  $10^{-12} \text{ s}^{-2}$  (Visser 2011; Bouman & Fuchs 2012), that is  $1 \text{ mE}$  ('E' denotes Eötvös unit;  $1 \text{ E} = 10^{-9} \text{ s}^{-2}$ ;  $1 \text{ mE} = 10^{-3} \text{ E}$ ). With a view of gravity forward modeling, a suitable gravity gradient calculation method must ensure that the modeling error is always less than the measurement error. Aware that the uncertainty still present in the Earth's geophysical models must be reduced further in order to be used with GOCE data, we still contend that the development of a reliable gravity gradient calculation method is a necessary first step. Thus, in order to be used with GOCE gravity gradients, the method should achieve at least an accuracy of a tenth or indeed a hundredth of millieötvös.

The paper is organized as follows: in Section 2, we review the definitions of fundamental physical quantities related to the gravity field. Section 3 is devoted to validating the numerical integration method from the comparison between the gravity field values of simple sources obtained by means of numerical and analytical calculations, respectively. The necessary mathematical background for understanding GLQ is recalled at this point. Section 4 outlines comparisons between the gravity gradient anomalies of an ellipsoidally shaped Earth, by means of spherical prism and ellipsoidal prism decompositions, respectively. The comparison is conducted in two cases, the first involving the density distribution given by the Preliminary Reference Earth Model (PREM; Dziewonski & Anderson 1981), the second using a combined density distribution derived from those given by LITHO1.0 and PREM.

## 2 THEORY

In this section, we provide notations and review the necessary mathematical background related to the gravity field. Only equations are written out, numerical tests for assessing our method will be presented in Section 3. The reasoning and mathematical approach adopted here are deliberately close to the ones of Asgharzadeh *et al.* (2007) for the purpose of comparison.

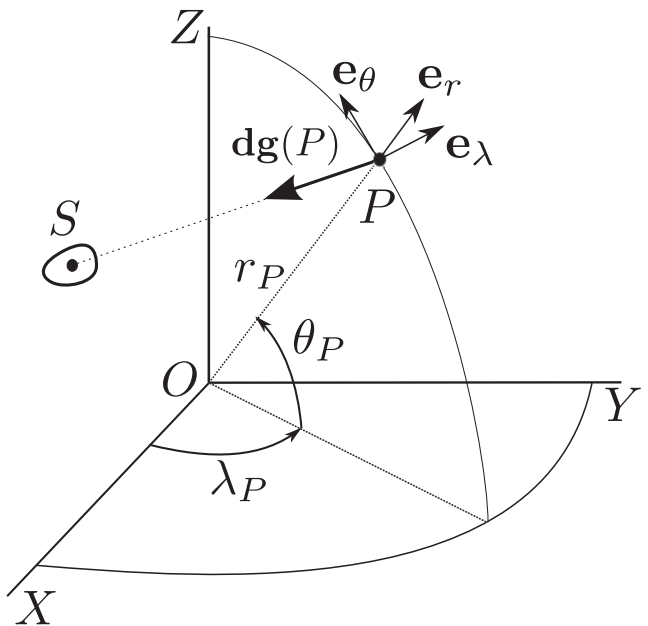


**Figure 1.** Gravity field of a mass source and spherical coordinate definition. The acceleration vector  $\mathbf{dg}(P)$  at the point  $P$  results from the gravitational attraction exerted by the mass source located at the point  $S$ . The frame  $(OXYZ)$  defines an Earth-fixed, Earth-centred, Cartesian reference frame. The observation point is positioned in the spherical coordinates  $(\lambda_P, \theta_P, r_P)$  consisting of the longitude  $\lambda_P$ , the spherical latitude  $\theta_P$  and the geocentric radius  $r_P$ . The set of vectors  $(\mathbf{e}_\lambda, \mathbf{e}_\theta, \mathbf{e}_r)$  is the local spherical basis at point  $P$ .

### 2.1 Gravity effects for a point mass

The gravitational potential  $dV(P)$  produced by a point pole ( $S$ ) of mass  $dm_S$  (in kg) located at the source point  $S$ , at the observation point  $P$  (Fig. 1) is given by :

$$dV(P) = G \frac{dm_S}{PS}, \quad (1)$$

where  $G$  is the gravitational constant ( $6.67 \cdot 10^{-11} \text{ m}^3 \text{ kg}^{-1} \text{ s}^{-2}$ ) and  $PS$  is the distance (in m) between the source point  $S$  and the observation point  $P$ . The gravitational acceleration vector  $\mathbf{dg}(P)$  (in  $\text{m s}^{-2} = 10^5 \text{ mGal}$ ) is obtained by calculating the space gradient vector of the scalar potential with respect to the point  $P$ :

$$\mathbf{dg}(P) = \nabla(dV(P)) = \nabla \left( G \frac{dm_S}{PS} \right). \quad (2)$$

In the remainder of the paper, only gravitational effects contributing to the Earth's gravity field will be accounted for and thus vector  $\mathbf{dg}(P)$  will be regarded as an infinitesimal element of the Earth's gravity vector. Finally, the gravity gradient tensor, also referred to as Marussi's tensor (in  $\text{s}^{-2} = 10^9 \text{ E}$ ), is obtained by calculating the tensor of space gradients of the gravity vector:

$$dT(P) = \nabla(\mathbf{dg}(P)) = \nabla(\nabla(V(P))) = \nabla \left( \nabla \left( G \frac{dm_S}{PS} \right) \right). \quad (3)$$

### 2.2 Gravity effects for an extended mass distribution

Let  $\rho_S$  be the constant density of the mass source of volume  $d\Omega_S$ ,  $\rho_S = dm_S/d\Omega_S$  (in  $\text{kg m}^{-3}$ ), then the point mass gravity effects given by eqs (1), (2) and (3), respectively become:

$$dV(P) = G \frac{\rho_S d\Omega_S}{PS}, \quad (4)$$

$$dg(P) = \nabla \left( G \frac{\rho_s d\Omega_s}{PS} \right) = G \nabla \left( \frac{1}{PS} \right) \rho_s d\Omega_s, \quad (5)$$

$$dT(P) = \nabla \left( \nabla \left( G \frac{\rho_s d\Omega_s}{PS} \right) \right) = G \nabla \left( \nabla \left( \frac{1}{PS} \right) \right) \rho_s d\Omega_s. \quad (6)$$

Hence, the gravity effects of an extended mass body may be expressed by integrating the gravity effects of the mass elements that fill up the volume  $\Omega$  of the body, thus giving:

$$V(P) = G \rho_s \int \int \int_{\Omega} \frac{d\Omega_s}{PS}, \quad (7)$$

$$g(P) = G \rho_s \int \int \int_{\Omega} \nabla \left( \frac{1}{PS} \right) d\Omega_s, \quad (8)$$

$$T(P) = G \rho_s \int \int \int_{\Omega} \nabla \left( \nabla \left( \frac{1}{PS} \right) \right) d\Omega_s. \quad (9)$$

The integrals in eqs (7)–(9) can be calculated once a first space coordinate system is chosen to locate the observation point  $P$  and a second to locate and describe the points  $S$  of the mass body ( $S$ ). On the one hand, when both are located by their Cartesian coordinates  $(X, Y, Z)$ , the mass bodies can be decomposed into rectangular prisms (right rectangular parallelepipeds) and integrals (7)–(9) can be expressed analytically, thus giving rigorous and consistent analytical forms describing the different gravity-related quantities (Nagy *et al.* 2000; Plouff 1976). On the other hand, when both are located by their spherical coordinates  $(\lambda, \theta, r)$  (Figs 1 and 2), the mass bodies can be modeled by tesseroids (spherical prisms) and integrals (7), (8) and (9) cannot be solved analytically. The GLQ is then needed to obtain approximates of the different gravity-related quantities (Asgharzadeh *et al.* 2007). Due to the flattening of the

Earth at the Poles, an approximation error occurs when one uses the spherical prism for describing large-scale geological structures within an ellipsoidal Earth. This will be investigated in Section 4. At this point, the mass element likely to be most suitable for decomposing ellipsoidal mass bodies is the ellipsoidal prism described subsequently.

## 2.3 Gravity effects for the ellipsoidal prism

### 2.3.1 Ellipsoidal coordinates

A reference ellipsoid of revolution about polar axis is commonly used to depict the Earth's shape as flattened at the Poles (oblate spheroid, see Fig. 3). Such an ellipsoid has two axes of equal length and a third shorter one. Its geometric properties are completely determined by its semi-major axis  $a$  (in m) and its eccentricity  $e$ . Let  $O$  be the centre of the ellipsoid and  $(OX)$ ,  $(OY)$ ,  $(OZ)$  the three axes of an orthogonal, right-handed Cartesian reference frame such that  $(OZ)$  coincides with the symmetry axis (polar axis) of the ellipsoid. In this case, the Cartesian coordinates  $(X_S, Y_S, Z_S)$  of any point  $S$  belonging to the ellipsoid denoted by  $\epsilon_{a,e}$  satisfy the following equation:

$$\frac{X_S^2 + Y_S^2}{a^2} + \frac{Z_S^2}{b^2} = 1, \quad (10)$$

where  $b = a\sqrt{1 - e^2}$  is the semi-minor axis of the ellipsoid.

Let  $\lambda_S$  be the longitude of the point  $S$ , that is, the angle between the meridian plane of Greenwich and the meridian plane that passes through that point and  $\varphi_S$  the latitude of the point  $S$ , that is, the angle between the equatorial plane and the normal to the ellipsoid that passes through that point. In terms of geodetic latitude  $\varphi_S$  and

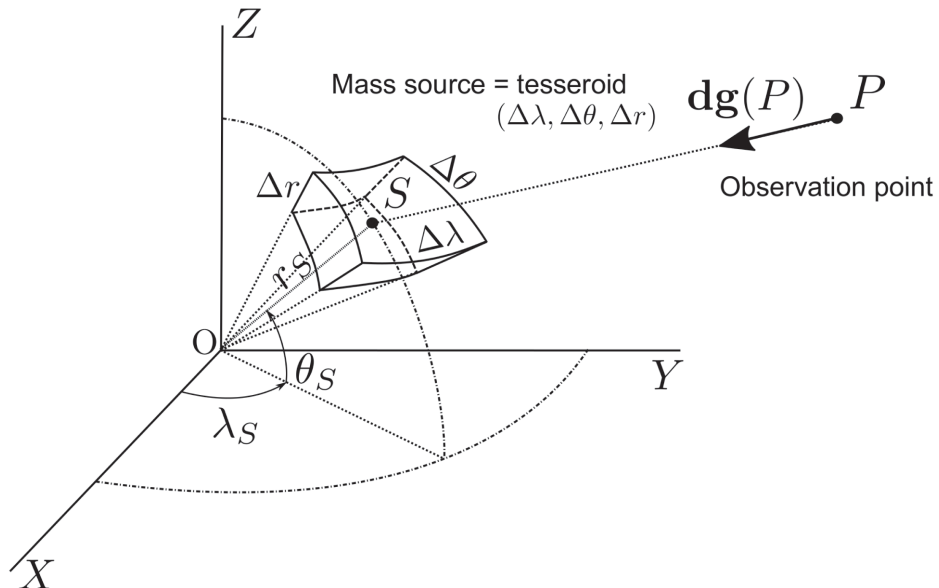


**Figure 2.** Tesseroid definition. When the points  $S$  of the Earth's body are located in the spherical coordinates  $(\lambda_S, \theta_S, r_S)$ , the mass element can be modeled by a spherical prism or 'tesseroid'. If the dimensions of the tesseroid are, respectively,  $\Delta\lambda$  for the longitude,  $\Delta\theta$  for the spherical latitude and  $\Delta r$  for the geocentric radius, then the tesseroid at point  $S$  corresponds to the mass element between the two meridians of respective longitudes  $\lambda_S - \Delta\lambda/2$  and  $\lambda_S + \Delta\lambda/2$ , the two conical surfaces leant on the parallels of respective latitudes  $\theta_S - \Delta\theta/2$  and  $\theta_S + \Delta\theta/2$  and the two geocentric spheres of respective radii  $r_S - \Delta r/2$  and  $r_S + \Delta r/2$ .

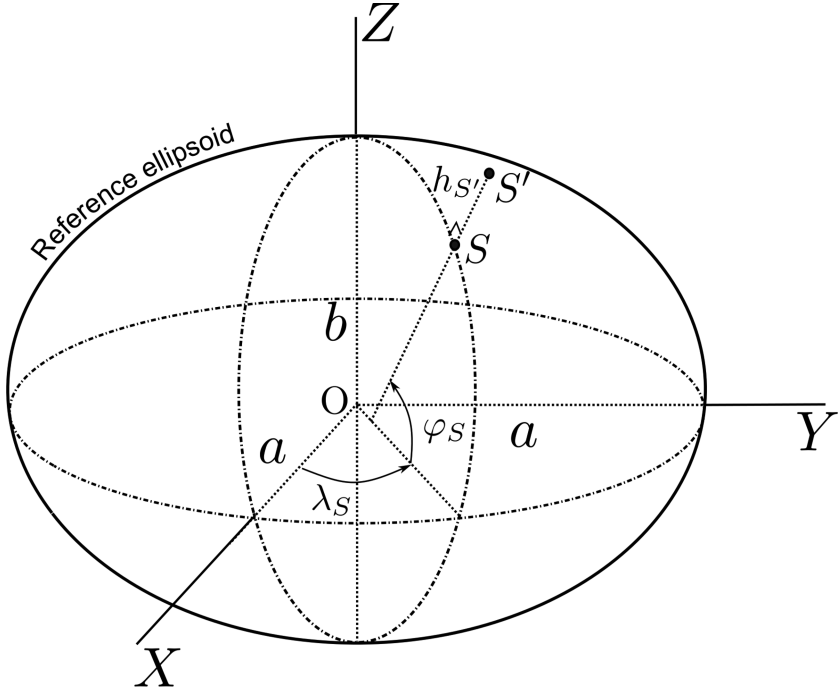


**Figure 3.** Reference ellipsoid and geodetic coordinates definitions. The reference ellipsoid of revolution about the polar axis ( $OZ$ ) is completely defined once given its semi-major axis  $a$  and its eccentricity  $e$ , from which the semi-minor axis  $b$  can be calculated. Any point  $S$  belonging to the reference ellipsoid can be positioned in the geodetic coordinates  $(\lambda_S, \varphi_S)$ . Any point  $S'$ , which does not belong to the ellipsoid surface, can still be located by using the algebraic distance  $h_{S'}$  measured between  $S'$  and  $S$  along the normal passing through  $S$ . The three numbers  $(\lambda_S, \varphi_S, h_{S'})$  thereby corresponds to the geodetic coordinates of point  $S'$ .

longitude  $\lambda_S$ , the Cartesian coordinates of point  $S$  may be expressed as:

$$\begin{cases} X_S = N_S(\varphi_S) \cos \varphi_S \cos \lambda_S \\ Y_S = N_S(\varphi_S) \cos \varphi_S \sin \lambda_S \\ Z_S = N_S(\varphi_S)(1 - e^2) \sin \varphi_S \end{cases}, \quad (11)$$

where  $N_S(\varphi_S)$  is the radius of curvature of the prime vertical at latitude  $\varphi_S$  given by:

$$N_S(\varphi_S) = \frac{a}{\sqrt{1 - e^2 \sin^2 \varphi_S}}. \quad (12)$$

Any point  $S'$  that does not belong to the ellipsoid surface can still be located given its ellipsoidal height  $h_{S'}$  (Fig. 3). The ellipsoidal height is the algebraic distance measured between  $S'$  and  $S$  along the normal that passes through  $S$ . The ellipsoid height  $h_{S'}$  of point  $S'$  can be either positive or negative depending on whether  $S'$  is located above or beneath the ellipsoid. Consequently, any point located on the ellipsoid surface has an ellipsoidal height equal to zero ( $h = 0$ ). Finally, the Cartesian coordinates  $(X_{S'}, Y_{S'}, Z_{S'})$  of the point  $S'$  are given by:

$$\begin{cases} X_{S'} = (N_S + h_{S'}) \cos \varphi_S \cos \lambda_S \\ Y_{S'} = (N_S + h_{S'}) \cos \varphi_S \sin \lambda_S \\ Z_{S'} = (N_S(1 - e^2) + h_{S'}) \sin \varphi_S \end{cases}. \quad (13)$$

The geodetic coordinates consisting of geodetic longitude and latitude completed by ellipsoidal height are commonly used to locate points with respect to a reference ellipsoid  $\epsilon_{a,e}$ . However, solving volume integrals such as those involved in gravity field calculations can actually be more conveniently achieved using another system of coordinates named ellipsoidal coordinates. Considering this coordinate system, the latitude and longitude of point  $S'$  previously

mentioned remain the same as those of its geodetic coordinates. A new coordinate denoted by  $u_{S'}$  replaces the ellipsoidal height  $h_{S'}$ , which may be expressed as a function of the Cartesian coordinates of  $S'$  as:

$$u_{S'} = \sqrt{\frac{X_{S'}^2 + Y_{S'}^2}{a^2} + \frac{Z_{S'}^2}{b^2}}. \quad (14)$$

Rewriting eq. (14) after having divided each of its members by  $u_{S'} \neq 0$  leads to:

$$\sqrt{\frac{X_{S'}^2 + Y_{S'}^2}{(u_{S'} a)^2} + \frac{Z_{S'}^2}{(u_{S'} b)^2}} = 1. \quad (15)$$

This can be interpreted by the fact that the point  $S'$  belongs to the ellipsoid  $\epsilon_{a',e'}$  the semi-major and semi-minor axes of which are, respectively, given by  $a' = u_{S'} a$  and  $b' = u_{S'} b$ . Such an ellipsoid as  $\epsilon_{a',e'}$  and the reference ellipsoid  $\epsilon_{a,e}$  are simply homothetic with a scaling factor equal to  $u_{S'}$ . In other words, the third coordinate  $u_{S'}$  in the ellipsoidal coordinates  $(\lambda_S, \varphi_S, u_{S'})$  of the point  $S'$  corresponds to the scaling factor needed to transform the reference ellipsoid into a concentric ellipsoid passing through the point  $S'$ . Since  $e'^2 = \frac{a'^2 - b'^2}{a'^2} = \frac{u_{S'}^2(a^2 - b^2)}{u_{S'}^2 a^2} = e^2$ , we have  $e' = e$ . The eccentricity of the ellipsoid  $\epsilon_{a',e'}$  therefore remains the same as that of the reference ellipsoid. Any point  $S$  on the reference ellipsoid satisfies  $u_S = 1$ . The coordinate  $u_{S'}$  of a point  $S'$ , which does not belong to the reference ellipsoid surface, can be either greater or lower than 1 depending on whether the homothetic ellipsoid passing through  $S'$  is located inside or outside the reference ellipsoid. In the ellipsoidal coordinate system, the functions relating the ellipsoidal coordinates

$(\lambda, \varphi, u)$  of any point  $M$  to its Cartesian coordinates  $(X, Y, Z)$  are the following:

$$\begin{cases} X = uN(\varphi)\cos\varphi\cos\lambda \\ Y = uN(\varphi)\cos\varphi\sin\lambda \\ Z = uN(\varphi)(1 - e^2)\sin\varphi \end{cases}, \quad (16)$$

where  $N(\varphi) = \frac{a}{\sqrt{1 - e^2 \sin^2 \varphi}}$ .

These relationships can be considered as a parametric representation of the ellipsoid passing through the point  $M$ , of same centre as the reference ellipsoid  $\epsilon_{a,e}$  and deduced from it by a scaling factor equal to  $u$ . The use of ellipsoidal coordinates has proven to be much more convenient than geodetic coordinates for mathematically decomposing the volume of an ellipsoid. From a practical point of view, the calculation of the ellipsoidal coordinates  $(\lambda, \varphi, u)$  of a point from its geodetic coordinates  $(\lambda, \varphi, h)$  is crucial because the latter are those usually given in the Earth's geophysical models. This can be readily carried out by transforming geodetic coordinates  $(\lambda, \varphi, h)$  in Cartesian coordinates  $(X, Y, Z)$  through eqs (13), and by calculating the scale factor  $u$  by means of eq. (14).

### 2.3.2 The ellipsoidal prism

An ellipsoidal prism can be easily defined in the ellipsoidal coordinates. Indeed, given:

- (i) two meridians of longitudes  $\lambda_1$  and  $\lambda_2$  respectively,
- (ii) two parallels of geodetic latitudes  $\varphi_1$  and  $\varphi_2$  respectively,
- (iii) two homothetic ellipsoids with the scaling factors  $u_1$  and  $u_2$  respectively,
- (iv) a constant density  $\rho_s$ ,

we obtain a unique ellipsoidal prism that can be viewed as the elementary solid body bounded by six surfaces (Fig. 4): the two

meridian planes of respective longitudes  $\lambda_1$  and  $\lambda_2$  ( $\lambda_1 < \lambda < \lambda_2$ ), the two conical surface formed by the lines that pass through point  $O$  and each point of the parallel circles of geodetic latitudes  $\varphi_1$  and  $\varphi_2$  ( $\varphi_1 < \varphi < \varphi_2$ ) respectively, and the surfaces of two geocentric and homothetic ellipsoids of respective scaling factors  $u_1$  and  $u_2$  ( $u_1 < u < u_2$ ). The prism volume can be infinitesimal if the differences  $\lambda_2 - \lambda_1$ ,  $\varphi_2 - \varphi_1$  and  $u_2 - u_1$  either are or are assumed to be infinitesimal themselves. In the context of gravity effect calculations, such bodies can be considered as ellipsoidal mass elements of constant density  $\rho_s$  and volume  $d\Omega_S$ . We shall now express the differential volume in the ellipsoidal coordinates, that is the volume  $d\Omega_S$  of an infinitesimal ellipsoidal prism centred at the point  $S(\lambda, \varphi, u)$ . This volume is mathematically given by Kellogg (1954):

$$d\Omega = |\det \mathbf{J}| d\lambda d\varphi du, \quad (17)$$

where  $\mathbf{J}$  is the Jacobian matrix of the parametric representation (16).

We have then to determine the Jacobian matrix given by:

$$\mathbf{J} = \begin{bmatrix} \partial_\lambda X & \partial_\varphi X & \partial_u X \\ \partial_\lambda Y & \partial_\varphi Y & \partial_u Y \\ \partial_\lambda Z & \partial_\varphi Z & \partial_u Z \end{bmatrix}, \quad (18)$$

where  $\partial_\alpha \dots, \alpha = \lambda, \varphi, u$  denotes the partial derivation with respect to  $\alpha$ .

After having performed all the calculations, we obtain:

$$d\Omega_S = \frac{a^3 \cos \varphi (1 - e^2) u^2}{[1 - e^2 \sin^2 \varphi]^{\frac{3}{2}}} d\lambda d\varphi du. \quad (19)$$

If we integrate this expression over the reference ellipsoid  $\epsilon_{a,e}$  for which the ellipsoidal coordinates  $\lambda, \varphi$  and  $u$  lie, respectively, within

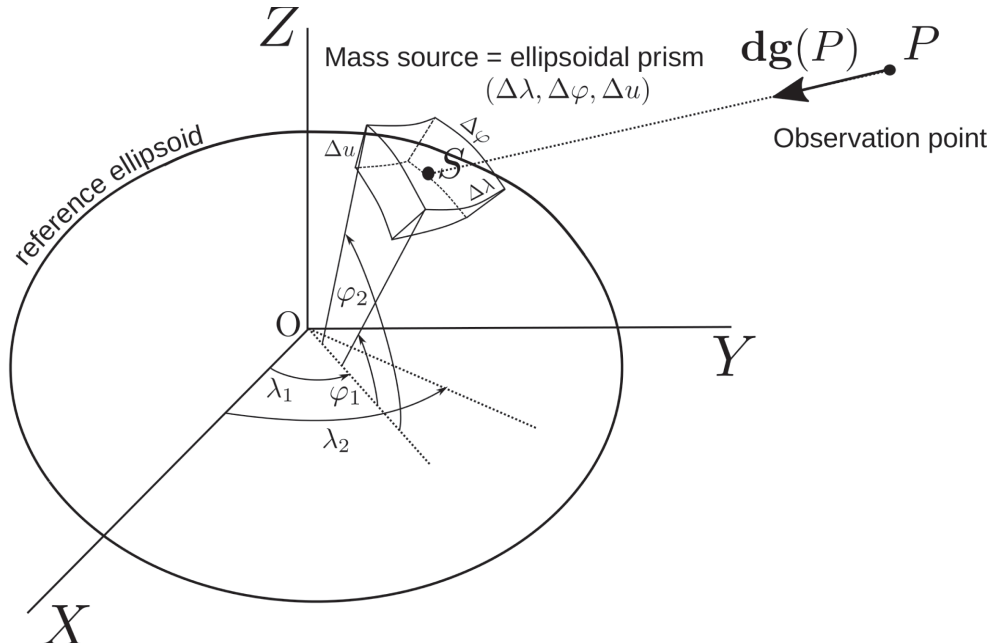


**Figure 4.** Ellipsoidal prism definition. The mass element bounded by the two meridian planes of longitudes  $\lambda_1$  and  $\lambda_2$ , respectively, the two conical surfaces formed by the lines passing through point  $O$  and each point of the parallel circles of geodetic latitudes  $\varphi_1$  and  $\varphi_2$ , respectively, and the surfaces of the two geocentric and homothetic ellipsoids of scale factors  $u_1$  and  $u_2$ , respectively, corresponds to an elementary ellipsoidal prism. The scale factors  $u_1$  and  $u_2$  are particularly derived from the two heights  $h_1$  and  $h_2$  commonly used in the Earth geophysical models to define the vertical boundaries of the mass elements.

$[0, 2\pi]$ ,  $[-\pi/2, \pi/2]$  and  $[0, 1]$ , then we can calculate its volume by:

$$\begin{aligned}\Omega_{e_{a,e}} &= \int_{\lambda=0}^{\lambda=2\pi} \int_{\varphi=-\frac{\pi}{2}}^{\varphi=\frac{\pi}{2}} \int_{u=0}^{u=1} \frac{a^3(1-e^2)\cos\varphi u^2}{(1-e^2\sin^2\varphi)^{\frac{3}{2}}} d\lambda d\varphi du \\ \Omega_{e_{a,e}} &= a^3(1-e^2)[\lambda]_0^{2\pi} \left[ \frac{u^3}{3} \right]_0^1 \left[ \frac{\sin\varphi}{\sqrt{1-e^2\sin^2\varphi}} \right]_{-\frac{\pi}{2}}^{\frac{\pi}{2}} \\ \Omega_{e_{a,e}} &= \frac{4\pi}{3}a^3\sqrt{1-e^2} = \frac{4\pi}{3}a^2b.\end{aligned}\quad (20)$$

Eq. (20) corresponds to the well-known formula giving the volume of an oblate spheroid the distinct axis lengths of which are, respectively,  $a$  and  $b$ .

### 2.3.3 Formulae for the ellipsoidal prism

To solve the integrals (7), (8) and (9), we still have to determine the expression of the distance  $PS$ . Since the mass  $S$  is now an ellipsoidal prism, the distance  $PS$  must be regarded as the distance between the observation point  $P$  and any point  $S$  located inside the ellipsoidal prism.

In order to obtain gravity field components in the local spherical basis, the observation point  $P$  is defined through its spherical coordinates  $(\lambda_P, \theta_P, r_P)$ , where  $\lambda_P$  is the longitude measured in the equatorial plane between the Greenwich meridian and the meridian plane passing through  $P$ ,  $\theta_P$  is the spherical latitude measured in the meridian plane between the equatorial plane and the radius vector  $\mathbf{r}_P$  from the Earth centre  $O$  to  $P$  and  $r_P$  is the magnitude of the radius vector  $\mathbf{r}_P$  (Fig. 1). Let  $(\lambda_S, \varphi_S, u_S)$  be the ellipsoidal coordinates of the running point  $S$  inside the ellipsoid. We can then express the distance  $PS$  as:

$$PS = \sqrt{\Delta X_{PS}^2 + \Delta Y_{PS}^2 + \Delta Z_{PS}^2}, \quad (21)$$

where:

$$\begin{aligned}\Delta X_{PS} &= X_P - X_S \\ \Delta Y_{PS} &= Y_P - Y_S \\ \Delta Z_{PS} &= Z_P - Z_S\end{aligned}\quad (22)$$

$$S \begin{cases} X_S = u_S N_S \cos \varphi_S \cos \lambda_S \\ Y_S = u_S N_S \cos \varphi_S \sin \lambda_S \\ Z_S = u_S N_S (1 - e^2) \sin \varphi_S \end{cases}, \quad (23)$$

using  $N_S(\varphi_S) = \frac{a}{\sqrt{1-e^2\sin^2\varphi_S}}$ , and,

$$P \begin{cases} X_P = r_P \cos \theta_P \cos \lambda_P \\ Y_P = r_P \cos \theta_P \sin \lambda_P \\ Z_P = r_P \sin \theta_P \end{cases}. \quad (24)$$

By substituting the above details into eq. (7), we obtain an integral form of the gravity potential produced by the ellipsoidal prism expressed as:

$$\begin{aligned}V(P) &= G \rho_S \int \int \int_{\Omega} \frac{d\Omega_S}{PS} \\ &= G \rho_S \int_{\lambda_1}^{\lambda_2} \int_{\varphi_1}^{\varphi_2} \int_{u_1}^{u_2} \frac{N_S^3 \cos \varphi_S (1 - e^2) u_S^2}{\sqrt{\Delta X_{PS}^2 + \Delta Y_{PS}^2 + \Delta Z_{PS}^2}} d\lambda_S d\varphi_S du_S.\end{aligned}\quad (25)$$

At this point, the derivation of the gravity vector components and gravity gradient tensor elements could have been performed in the local ellipsoidal basis at point  $P$ . As previously mentioned, since we are interested of having the gravity vector and the gravity gradient tensor expressed in the local spherical basis, the gradient operator  $\nabla$  has to be expressed in the spherical coordinates. This operator has three components measured in the local spherical basis  $(\mathbf{e}_{\lambda}, \mathbf{e}_{\theta}, \mathbf{e}_r)$  consisting of three unitary, two-by-two orthogonal vectors, each having its origin at point  $P$ . Let  $(g_{\lambda}, g_{\theta}, g_r)$  be the components of the gravity vector given by eq. (8) in the local spherical basis, that is:

$$\mathbf{g}(P) = g_{\lambda} \mathbf{e}_{\lambda} + g_{\theta} \mathbf{e}_{\theta} + g_r \mathbf{e}_r; \quad (26)$$

then we have:

$$g_{\lambda}(P) = G \rho_S \int \int \int_{\Omega} \frac{1}{r_P \cos \theta_P} \frac{\partial}{\partial \lambda_P} \left( \frac{1}{PS} \right) d\Omega_S, \quad (27)$$

$$g_{\theta}(P) = G \rho_S \int \int \int_{\Omega} \frac{1}{r_P} \frac{\partial}{\partial \theta_P} \left( \frac{1}{PS} \right) d\Omega_S, \quad (28)$$

$$g_r(P) = G \rho_S \int \int \int_{\Omega} \frac{\partial}{\partial r_P} \left( \frac{1}{PS} \right) d\Omega_S. \quad (29)$$

Similarly, by substituting the above-mentioned details, we obtain integral forms of the gravity vector components:

$$g_{\lambda}(P) = G \rho_S \int_{\lambda_1}^{\lambda_2} \int_{\varphi_1}^{\varphi_2} \int_{u_1}^{u_2} \frac{X_P Y_S - Y_P X_S}{r_P \cos \theta_P PS^3} d\Omega_S, \quad (30)$$

$$g_{\theta}(P) = G \rho_S \int_{\lambda_1}^{\lambda_2} \int_{\varphi_1}^{\varphi_2} \int_{u_1}^{u_2} \times \frac{Z_P (\cos \lambda_P \Delta X_{PS} + \sin \lambda_P \Delta Y_{PS}) - r_P \cos \theta_P \Delta Z_{PS}}{r_P PS^3} d\Omega_S, \quad (31)$$

$$g_r(P) = -G \rho_S \int_{\lambda_1}^{\lambda_2} \int_{\varphi_1}^{\varphi_2} \int_{u_1}^{u_2} \times \frac{X_P \Delta X_{PS} + Y_P \Delta Y_{PS} + Z_P \Delta Z_{PS}}{r_P PS^3} d\Omega_S, \quad (32)$$

where  $d\Omega_S = N_S^3 \cos \varphi_S (1 - e^2) u^2 d\lambda d\varphi du$ .

Finally, the elementary gravity gradient tensor  $dT$  defined by eq. (3) may be expressed in the local spherical basis as the elements of a  $3 \times 3$  square matrix as follows:

$$dT = \begin{bmatrix} dT_{\lambda\lambda} & dT_{\lambda\theta} & dT_{\lambda r} \\ dT_{\theta\lambda} & dT_{\theta\theta} & dT_{\theta r} \\ dT_{r\lambda} & dT_{r\theta} & dT_{rr} \end{bmatrix}. \quad (33)$$

By incorporating the previous details into the gravity gradient components, we obtain the expressions given in Table 1 and the related partial derivatives given in Table 2. The complete gravity gradient tensor  $T$  results from the integration of the elements of  $dT$  over the source volume. Each of its elements may be expressed as:

$$T_{vw} = \int \int \int_{\Omega} dT_{vw} = \int_{\lambda_1}^{\lambda_2} \int_{\varphi_1}^{\varphi_2} \int_{u_1}^{u_2} dT_{vw} \quad (34)$$

where  $v, w = r, \theta$  or  $\lambda$ .

**Table 1.** Gravity gradient tensor elements.

Element	Expression
$dT_{\lambda\lambda}$	$\frac{1}{r_P \cos \theta_P} \frac{\partial(dg_\lambda)}{\partial \lambda_P} + \frac{1}{r_P} dg_r - \frac{\sin \theta_P}{r_P \cos \theta_P} dg_\theta$
$dT_{\lambda\theta}$	$\frac{1}{r_P} \frac{\partial(dg_\lambda)}{\partial \theta_P}$
$dT_{\lambda r}$	$\frac{\partial(dg_\lambda)}{\partial r_P}$
$dT_{\theta\lambda}$	$\frac{1}{r_P \cos \theta_P} \frac{\partial(dg_\theta)}{\partial \lambda_P} + \frac{\sin \theta_P}{r_P \cos \theta_P} dg_\lambda$
$dT_{\theta\theta}$	$\frac{1}{r_P} \frac{\partial(dg_\theta)}{\partial \theta_P} + \frac{1}{r_P} dg_r$
$dT_{\theta r}$	$\frac{\partial(dg_\theta)}{\partial r_P}$
$dT_{r\lambda}$	$\frac{1}{r_P \cos \theta_P} \frac{\partial(dg_r)}{\partial \lambda_P} - \frac{1}{r_P} dg_\lambda$
$dT_{r\theta}$	$\frac{1}{r_P} \frac{\partial(dg_r)}{\partial \theta_P} - \frac{1}{r_P} dg_\theta$
$dT_{rr}$	$\frac{\partial(dg_r)}{\partial r_P}$

Note. The nine elements of the gradient gravity tensor expressed in the local spherical basis, tabulated as functions of the gravity vector components.

Finally, it should be noted that the local spherical basis defined in this manuscript (Fig. 1) and the LNOF mentioned in the introduction are different. The transformation between these two frames simply involves a matrix such as:

$$Q = R_3(90^\circ) = \begin{pmatrix} 0 & 1 & 0 \\ -1 & 0 & 0 \\ 0 & 0 & 1 \end{pmatrix}. \quad (35)$$

If  $T$  is the gravity gradient tensor expressed in the local spherical basis and  $T^{\text{LNOF}}$  is the gravity gradient tensor expressed in the LNOF, then:

$$T^{\text{LNOF}} = Q T Q^T. \quad (36)$$

**Table 2.** Partial derivatives of gravity vector components.

Element	Expression
$\frac{\partial(dg_\lambda)}{\partial \lambda_P}$	$G\rho_S \left[ \frac{3(Y_P X_S - X_P Y_S)^2}{r_P \cos \theta_P P S^5} + \frac{X_P \Delta X_{PS} + Y_P \Delta Y_{PS} - r_P^2 \cos^2 \theta_P}{r_P \cos \theta_P P S^3} \right] d\Omega_S$
$\frac{\partial(dg_\lambda)}{\partial \theta_P}$	$G\rho_S \left[ \frac{Z_P (\cos \lambda_P \Delta Y_{PS} - \sin \lambda_P \Delta X_{PS}) + \sin \theta_P (X_P Y_S - Y_P X_S)}{r_P \cos \theta_P P S^3} + \dots \right. \\ \left. \dots \frac{3(X_P Y_S - Y_P X_S)(Z_P (\cos \lambda_P \Delta X_{PS} + \sin \lambda_P \Delta Y_{PS}) - r_P \cos \theta_P \Delta Z_{PS})}{r_P \cos \theta_P P S^5} \right] d\Omega_S$
$\frac{\partial(dg_\lambda)}{\partial r_P}$	$G\rho_S \left[ \frac{3(Y_P X_S - X_P Y_S)(X_P \Delta X_{PS} + Y_P \Delta Y_{PS} + Z_P \Delta Z_{PS})}{r_P^2 \cos \theta_P P S^5} \right] d\Omega_S$
$\frac{\partial(dg_\theta)}{\partial \lambda_P}$	$G\rho_S \left[ \frac{3(X_P Y_S - Y_P X_S)(Z_P (\cos \lambda_P \Delta X_{PS} + \sin \lambda_P \Delta Y_{PS}) - r_P \cos \theta_P \Delta Z_{PS})}{r_P \cos \theta_P P S^5} + \dots \right. \\ \left. \dots \frac{Z_P (\cos \lambda_P \Delta Y_{PS} - \sin \lambda_P \Delta X_{PS})}{r_P P S^3} \right] d\Omega_S$
$\frac{\partial(dg_\theta)}{\partial \theta_P}$	$G\rho_S \left[ \frac{3(Z_P (\cos \lambda_P \Delta + \sin \lambda_P \Delta Y_{PS}) - r_P \cos \theta_P \Delta Z_{PS})^2}{r_P P S^5} + \frac{X_P \Delta X_{PS} + Y_P \Delta Y_{PS} + Z_P \Delta Z_{PS} - r_P^2}{r_P P S^3} \right] d\Omega_S$
$\frac{\partial(dg_\theta)}{\partial r_P}$	$G\rho_S \left[ \frac{3(r_P \cos \theta_P \Delta Z_{PS} - Z_P (\sin \lambda_P \Delta Y_{PS} + \cos \lambda_P \Delta X_{PS}))(X_P \Delta X_{PS} + Y_P \Delta Y_{PS} + Z_P \Delta Z_{PS})}{r_P^2 P S^5} \right] d\Omega_S$
$\frac{\partial(dg_r)}{\partial \lambda_P}$	$G\rho_S \left[ \frac{3(Y_P X_S - X_P Y_S)(X_P \Delta X_{PS} + Y_P \Delta Y_{PS} + Z_P \Delta Z_{PS})}{r_P P S^5} - \frac{Y_P X_S - X_P Y_S}{r_P P S^3} \right] d\Omega_S$
$\frac{\partial(dg_r)}{\partial \theta_P}$	$G\rho_S \left[ \frac{(r_P \cos \theta_P \Delta Z_{PS} - Z_P (\cos \lambda_P \Delta X_{PS} + \sin \lambda_P \Delta Y_{PS})) (3(X_P \Delta X_{PS} + Y_P \Delta Y_{PS} + Z_P \Delta Z_{PS}) - P S^2)}{r_P P S^5} \right] d\Omega_S$
$\frac{\partial(dg_r)}{\partial r_P}$	$G\rho_S \left[ \frac{3(X_P \Delta X_{PS} + Y_P \Delta Y_{PS} + Z_P \Delta Z_{PS})^2}{r_P^2 P S^5} - \frac{1}{P S^3} \right] d\Omega_S$

Note. Partial derivatives of the three elementary gravity vector components involved in the expressions of gravity gradient tensor elements (Table 1), expressed in the local spherical basis.

### 3 ASSESSMENT OF THE NUMERICAL INTEGRATION METHOD

#### 3.1 The Gauss–Legendre quadrature

Integrating eqs (7)–(9) analytically is quite complicated. Instead we evaluate them using the GLQ. Specifically, these integrals can be expressed as the generalized triple integral:

$$\int_{\lambda_1}^{\lambda_2} \int_{\varphi_1}^{\varphi_2} \int_{u_1}^{u_2} f(\lambda_P, \theta_P, r_P, \lambda_S, \varphi_S, u_S) du_S d\varphi_S d\lambda_S, \quad (37)$$

which can be numerically evaluated by means of the following quadrature formula:

$$\frac{(\lambda_2 - \lambda_1)(\varphi_2 - \varphi_1)(u_2 - u_1)}{8} \sum_{i=1}^{n_\lambda} \sum_{j=1}^{n_\varphi} \sum_{k=1}^{n_u} \times \omega_i \omega_j \omega_k f(\lambda_P, \theta_P, r_P, \lambda_{S_i}, \varphi_{S_j}, u_{S_k}), \quad (38)$$

where the function  $f$  is calculated at  $n_\lambda \times n_\varphi \times n_u$  optimal points, also called nodes, and each corresponding value is weighted by the product of three Gauss–Legendre coefficients (or weights)  $\omega_i$ ,  $\omega_j$  and  $\omega_k$ . Prior to the calculation of the quadrature formula (38), the ellipsoidal coordinates  $(\lambda_{S_i}, \varphi_{S_j}, u_{S_k})$  of the nodes and the corresponding weights have to be determined. The determination method is easily outlined by considering one single coordinate,  $\lambda_{S_i}$  for instance. This coordinate is simply related to the  $i$ th root  $\hat{\lambda}_{S_i}$  of the  $n_\lambda$ th order polynomial  $P_{n_\lambda}$  from the set of orthogonal Legendre polynomials defined over the range  $[-1, +1]$ , by Asgharzadeh *et al.* (2007):

$$\lambda_{S_i} = \frac{\lambda_1 + \lambda_2}{2} + \hat{\lambda}_{S_i} \frac{\lambda_2 - \lambda_1}{2}, \quad (39)$$

where  $\hat{\lambda}_{S_i}$  lies within  $[-1, +1]$ .

The weight  $\omega_i$  affected to the coordinate  $\lambda_{S_i}$  is then given by:

$$\omega_i = \frac{2}{n_\lambda P_{n_\lambda-1}(\hat{\lambda}_{S_i}) P'_{n_\lambda}(\hat{\lambda}_{S_i})}, \quad (40)$$

where  $P_{n_\lambda-1}$  is the  $(n_\lambda - 1)$ th-order Legendre polynomials and  $P'_{n_\lambda}$  the first derivative of  $P_{n_\lambda}$ .

The remaining coordinates and weights can be calculated similarly by means of the same method, thus giving:

$$\varphi_{S_j} = \frac{\varphi_1 + \varphi_2}{2} + \hat{\varphi}_{S_j} \frac{\varphi_2 - \varphi_1}{2}, \quad P_{n_\varphi}(\hat{\varphi}_{S_j}) = 0, \\ \omega_j = \frac{2}{n_\varphi P_{n_\varphi-1}(\hat{\varphi}_{S_j}) P'_{n_\varphi}(\hat{\varphi}_{S_j})}; \quad (41)$$

$$u_{S_k} = \frac{u_1 + u_2}{2} + \hat{u}_{S_k} \frac{u_2 - u_1}{2}, \quad P_{n_u}(\hat{u}_{S_k}) = 0 \\ \omega_k = \frac{2}{n_u P_{n_u-1}(\hat{u}_{S_k}) P'_{n_u}(\hat{u}_{S_k})}. \quad (42)$$

The quadrature formula in eq. (38) shows that the complete gravity field of the ellipsoidal prism in eqs (7)–(9) can actually be computed by summing at each observation point the effects of  $n_\lambda \times n_\varphi \times n_u$  equivalent point poles (see Section 2), each located within the prism at the source point given in the ellipsoidal coordinates by  $(\lambda_{S_i}, \varphi_{S_i}, u_{S_i})$ , the gravity effect of which is weighted by the relevant Gauss–Legendre coefficients related to the  $(\lambda_S, \varphi_S, u_S)$  limits of the prism. The only issue remaining in applying eq. (38) is the selection of the number of nodes for the efficient computation of accurate gravity field values. A large number of nodes ensures a very accurate quadrature solution, but implies a longer computational time. The number of nodes will depend on the desired accuracy, the size of the ellipsoidal prism, the distance between the observation point and the prism and the gravity field constituent—gravitational potential, components of the gravity field vector, components of the gravity gradient tensor—to be computed. Concerning the calculation time, since our method only differs from that using spherical prisms (Asgharzadeh *et al.* 2007) by slightly more complex integrands, we do not observe really significant calculation time difference.

### 3.2 Validation of the Gauss–Legendre quadrature

To test whether the GLQ computation with ellipsoidal prisms gives reasonable estimates of the gravity gradients, we carried out numerical gravity gradient calculation for an ellipsoidal shell of constant density. In this particular case, true analytical formulae exist in the Cartesian coordinates (Kellogg 1954), thus allowing the gravity vector components and the Marussi's tensor elements specifically at any point in a local Cartesian basis to be calculated. Once expressed in the local spherical basis, these quantities are directly comparable to those provided by the GLQ and their differences measure the approximation error. Put more precisely, we considered the ellipsoidal shell located between two homothetical ellipsoids  $\epsilon_{u=1}$  and  $\epsilon_{u \approx 1.00157}$ , respectively, which is equivalent in terms of ellipsoidal height to an elevation of 10 km above the Equator and an elevation of about 9.966 km above the North and South Poles. The value of the density was deliberately set to  $10\,000 \text{ kg m}^{-3}$ . The choice of an outer shell and a high density value was made in order to obtain an upper limit of the error. The ellipsoidal layer was decomposed into a set of ellipsoidal prisms defined by:

- (i)  $u_{S_1} = 1$  and  $u_{S_2} \approx 1.00157$ .
- (ii)  $\Delta\lambda_S = \Delta\varphi_S = 1^\circ$ .

Overall, the ellipsoidal shell was divided into  $360 \times 180 = 64\,800$  ellipsoidal prisms. Finally, the gravity field has been computed ev-

ery  $1^\circ$  latitude above the meridian of  $0^\circ$  longitude from the Equator to the North Pole ( $0^\circ \leq \varphi < 90^\circ$ ) at an ellipsoidal height of 260 km. The GLQ was computed using orders equal to 3/3/2, that is, order 3 for longitudes and latitudes and order 2 for the scaling factor  $u_S$ . Computing the gravity effect of a unique prism thereby required summing of  $3 \times 3 \times 2 = 18$  effects of equivalent point poles located within it. For the purpose of comparison, calculations involving 2/2/2 and 4/4/4 orders were also performed. The graphs in Fig. 5 show the numerical error  $e_{T_{uv}}$  on the nine elements  $T_{uv}$ ,  $u, v = \lambda, \theta, r$  of the gravity gradient tensor as a function of the latitude. The numerical error  $e_{T_{uv}}$  corresponds to the difference between the values of  $T_{uv}$  provided, respectively, by GLQ and by means of analytical formulae. Notably, even though the gravity gradient tensor is symmetric ( $T_{uv} = T_{vu}$  for  $u \neq v$ ), the errors on both elements have been systematically calculated given that their expressions are actually different (*cf.* Tables 1 and 2).

As is made clear in Fig. 5, the errors that occur when using GLQ in the computation of gravity effects are in the order of tenth of millieötvös for orders 3/3/2 and higher, which complies with the desired accuracy—better than 1 mE. Such orders 3/3/2 have been chosen so as to ensure an adequate accuracy with a reasonable computation time. If appropriate, these orders must be changed depending on the location of observation points and the size of the prisms. Because of its revolution symmetry, the ellipsoidal layer produces gravity effects such as  $T_{\lambda\theta} = T_{\theta\lambda} = T_{\lambda r} = T_{r\lambda} = 0$ , which can have been estimated by GLQ at the same accuracy level. For a given set of orders, the accuracy of the GLQ can be significantly improved by using lower size prism. Take, as an example, the orders 3/3/2 with half-size prisms ( $\Delta\lambda_S = \Delta\varphi_S = 0.5^\circ$ ). As shown in Fig. 6, the error affecting the element  $T_{rr}$  regardless of the latitude is markedly lower than that obtained with  $1^\circ \times 1^\circ$  prisms using orders 4/4/4. These results indicates that, for given gravity sources, the gravity gradients at less than 1 mE uncertainty can be numerically computed at GOCE altitude using GLQ, provided that the number of nodes per prism or the prism size have been suitably chosen.

## 4 GEOPHYSICAL APPLICATION

We are interested in the computation of the gravity gradient anomalies from available geophysical models of the Earth's interior. The basic idea is that after calculating the gravity gradients at GOCE altitude we shall be able to compare the gravity anomaly values predicted by the geophysical models to those derived from GOCE measurements anywhere over the Earth's surface. If we were ever to refine the Earth's geophysical models at a global or local scale by means of GOCE data, we would first have to perform joint inversions involving both seismic and satellite gravity data in order to estimate the unknown densities inside the Earth. For this task, our calculation method for determining gravity gradients from Earth models actually solves the forward problem of density estimation under the assumption of an ellipsoidal Earth. Our aim is therefore to demonstrate the efficiency of the method for calculating the gravity gradient anomalies from any Earth model of ellipsoidal shape.

Geological models usually consist of physical properties of the Earth registered in elementary contiguous cells located on a regular geographical grid, where each node is defined by its geodetic coordinates. As shown in Fig. 7, it is then possible to construct

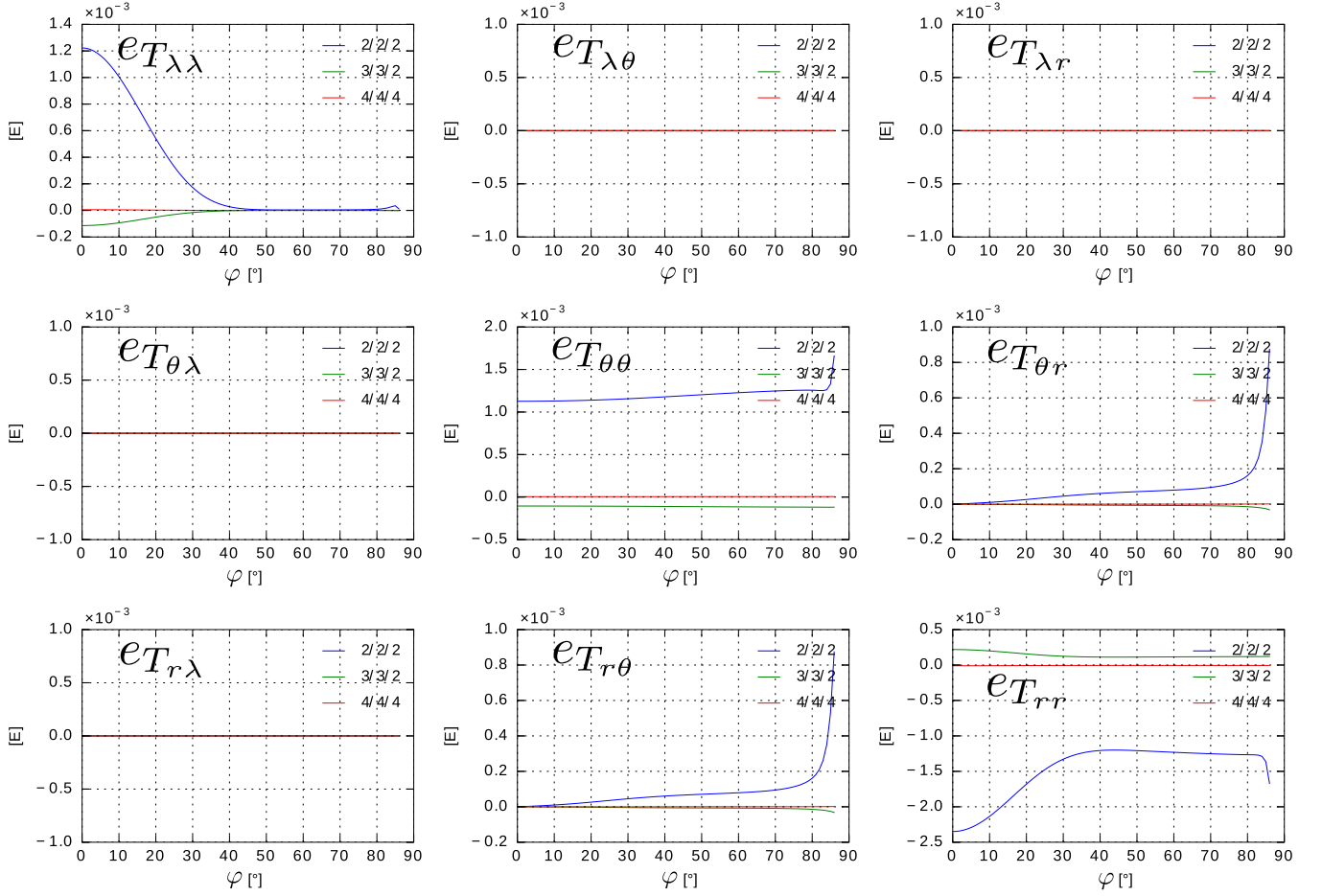


**Figure 5.** Approximation error on the gravity gradient tensor elements produced by a constant density ellipsoidal shell calculated by means of the GLQ. The error, which corresponds to the difference between the values provided, respectively, by the GLQ and analytical formulae, has been plotted for all elements of the gravity gradient tensor as a function of the latitude and for three sets of GLQ orders (2/2/2, 3/3/2, 4/4/4). The use of orders 3/3/2 in the GLQ allows the error to be maintained under one-tenth of millieötvös regardless of the latitude. Even less error can be achieved by means of orders 4/4/4 but requires a longer computation time.

the corresponding ellipsoidal and spherical prisms. Let us consider a unique cell of a geological grid model, which provides us with the location  $(\lambda, \varphi, h)$ , the size  $(\Delta\lambda, \Delta\varphi, \Delta h)$  and the density  $\rho$  of an elementary solid body. First, we can easily express the Cartesian coordinates  $(X_S, Y_S, Z_S)$  of its top centre ( $S$ ):

$$\begin{cases} X_S = (N + h) \cos \varphi \cos \lambda \\ Y_S = (N + h) \cos \varphi \sin \lambda \\ Z_S = (N(1 - e^2) + h) \sin \varphi \end{cases} \quad (43)$$

and the Cartesian coordinates  $(X'_{S'}, Y'_{S'}, Z'_{S'})$  of its bottom centre ( $S'$ ):

$$\begin{cases} X_{S'} = (N + (h + \Delta h)) \cos \varphi \cos \lambda \\ Y_{S'} = (N + (h + \Delta h)) \cos \varphi \sin \lambda \\ Z_{S'} = (N(1 - e^2) + (h + \Delta h)) \sin \varphi \end{cases} \quad (44)$$

As a reminder (see Section 2), the ellipsoidal prism is defined by two meridians of longitudes  $\lambda_1$  and  $\lambda_2$ , respectively, two parallels of geodetic latitudes  $\varphi_1$  and  $\varphi_2$ , respectively, and two homothetic

ellipsoids with the scaling factors  $u_1$  and  $u_2$ , respectively, given by:

$$\begin{cases} \lambda_1 = \lambda - \frac{\Delta\lambda}{2} & \lambda_2 = \lambda + \frac{\Delta\lambda}{2} \\ \varphi_1 = \varphi - \frac{\Delta\varphi}{2} & \varphi_2 = \varphi + \frac{\Delta\varphi}{2} \\ u_1 = \sqrt{\frac{X_{S'}^2 + Y_{S'}^2}{a^2} + \frac{Z_{S'}^2}{b^2}} & u_2 = \sqrt{\frac{X_S^2 + Y_S^2}{a^2} + \frac{Z_S^2}{b^2}} \end{cases}. \quad (45)$$

Its spherical counterpart is defined by two meridians of longitudes  $\lambda_1$  and  $\lambda_2$ , respectively, two parallels of geocentric latitudes  $\theta_1$  and  $\theta_2$ , respectively and two concentric spheres of radii  $r_1$  and  $r_2$ , respectively, given by:

$$\begin{cases} \lambda_1 = \lambda - \frac{\Delta\lambda}{2} & \lambda_2 = \lambda + \frac{\Delta\lambda}{2} \\ \theta_1 = \arctan((1 - e^2) \times \tan(\varphi - \frac{\Delta\varphi}{2})) & \theta_2 = \arctan((1 - e^2) \tan(\varphi + \frac{\Delta\varphi}{2})) \\ r_1 = \sqrt{X_{S'}^2 + Y_{S'}^2 + Z_{S'}^2} & r_2 = \sqrt{X_S^2 + Y_S^2 + Z_S^2} \end{cases}. \quad (46)$$

Note that, as their spherical counterparts, ellipsoidal prisms of same geodetic latitudes boundaries,  $\varphi_1$  and  $\varphi_2$ , are all included between the two geocentric latitudes  $\theta_1$  and  $\theta_2$  (Fig. 7). This property results from the conservation of the excentricity value  $e$  that has been demonstrated in Section 2. Once having solved the problem of numerically computing the gravity effects of an ellipsoidal prism, the next task is to compare the numerical values of gravity provided

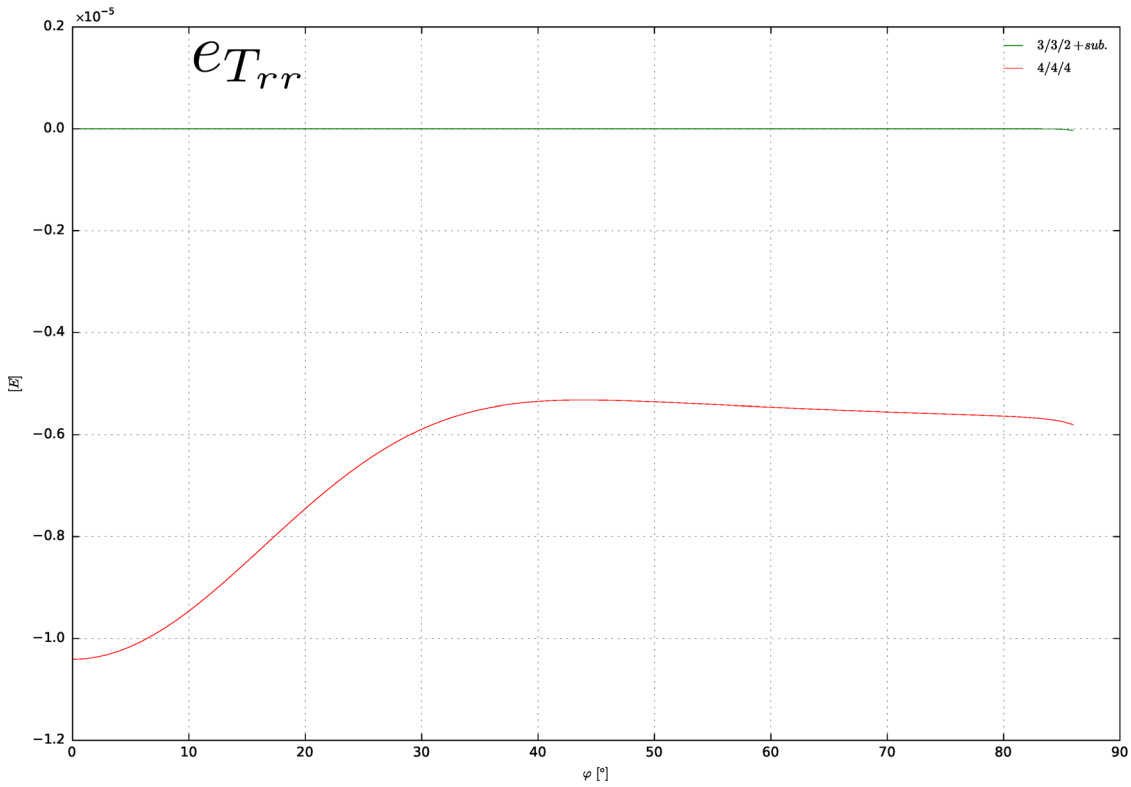


**Figure 6.** The graph shows the error that occurs on  $T_{rr}$  gravity tensor element with the orders 3/3/2 (green solid line) after dividing twofold the size of the ellipsoidal prism ( $\Delta\lambda = \Delta\varphi = 0.5^\circ$ ). The error is now negligible when compared to that obtained for  $1^\circ$  size prisms and the orders 4/4/4 (red solid line). The result suggests that a better accuracy in the GLQ computation can be achieved by a simple change of prism size.

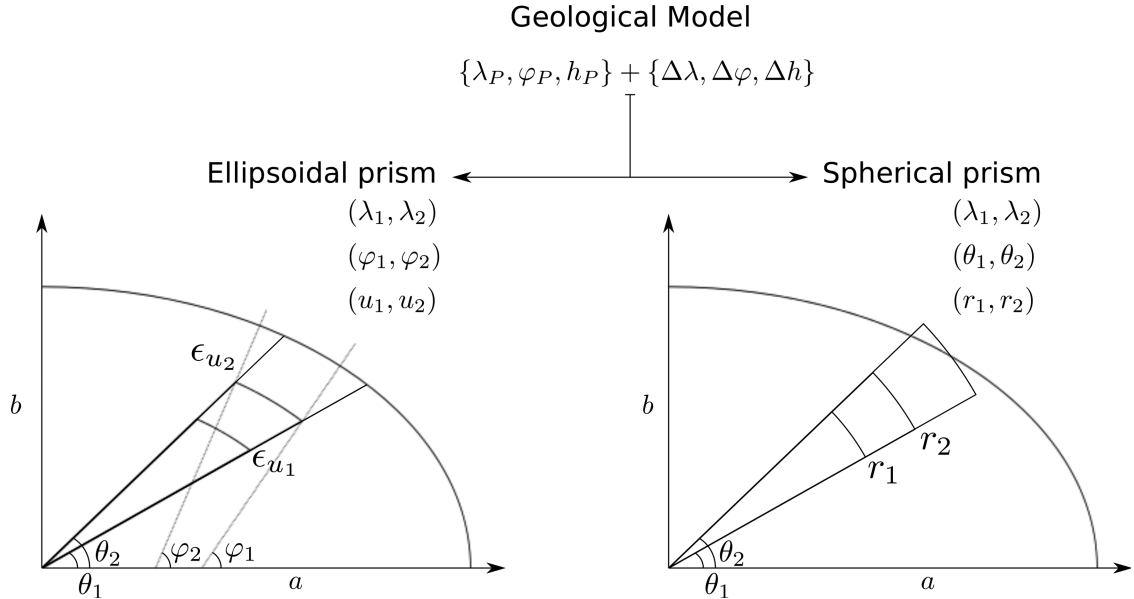


**Figure 7.** Geometrical construction of ellipsoidal and spherical prisms from geological model information. Geographical information contained in geological grid model is used to define the geometric location and boundaries of the ellipsoidal and spherical prisms.

by GLQ using spherical and ellipsoidal prisms for the discretization of an ellipsoidal shaped Earth.

#### 4.1 Effect of an improper mass estimation

According to Fig. 7, the ellipsoidal and spherical prisms are not perfectly stackable. Consequently, they do not represent the same

volume and by extension the same mass since they have the same density  $\rho$ . To assess the impact of equating ellipsoidal and spherical prisms on gravity gradient calculation, it is helpful to estimate the gravity gradient variation induced by a given variation of the gravity source mass. As typical of this variation, we shall consider the magnitude of the gravity gradient along the radial direction  $d\Omega_S$  produced at the point  $P$  by the mass element  $d\Omega_S$  located at the

point  $S$ . According to Tables 1 and 2, the magnitude  $dT_{rr}$  of the elementary tensor  $\mathbf{dT}$  is given by:

$$dT_{rr} = G\rho_S \frac{\partial^2}{\partial r_p^2} \left( \frac{1}{PS} \right) d\Omega_S. \quad (47)$$

Given the fact that the product  $\rho_S d\Omega_S$  correspond to the elementary mass of the source placed at  $S$ , the variation of the radial gradient magnitude per unit of mass  $\tau_{rr}$  due to the mass source at  $S$  may simply be expressed as:

$$\tau_{rr} = \frac{dT_{rr}}{\rho_S d\Omega_S} = G \frac{\partial^2}{\partial r_p^2} \left( \frac{1}{PS} \right). \quad (48)$$

This quantity depends only on the relative position of the observation point  $P$  with respect to the source point  $S$ , and the question then arises, how does it vary when the point  $S$  skims within the Earth's interior. A reasonable estimate of  $\tau_{rr}$  for the Earth at GOCE altitude can be obtained by calculating its mean value over the entire volume of a sphere  $\Sigma_T$  centred at the point  $O$  and of radius  $\bar{R}$ . This yields to:

$$\langle \tau_{rr} \rangle = \iiint_{\Sigma_T} G \frac{\partial^2}{\partial r_p^2} \left( \frac{1}{PS} \right) d\Omega_S, \quad (49)$$

which can be transformed by inverting the triple integration and the double differentiation which operate on independent variables, thus giving:

$$\langle \tau_{rr} \rangle = G \frac{\partial^2}{\partial r_p^2} \iiint_{\Sigma_T} \left( \frac{1}{PS} \right) d\Omega_S = G \frac{\partial^2}{\partial r_p^2} \left\langle \frac{1}{PS} \right\rangle. \quad (50)$$

For a point  $P$  located outside the sphere  $\Sigma_T$ , the mean value of the reciprocal distance  $\frac{1}{PS}$  is simply equal to  $\frac{1}{r_p}$ . After having performed the double differentiation with respect to  $r_p$ , we obtain finally:

$$\langle \tau_{rr} \rangle = \frac{2G}{r_p^3}. \quad (51)$$

Let us consider the satellite GOCE orbiting at  $h_{\text{GOCE}} = 260$  km height above the mean sphere of radius  $\bar{R} = 6371$  km such as  $r_p = h_{\text{GOCE}} + \bar{R}$ . This leads to an estimate of the radial gravity gradient variation per unit mass  $\langle \tau_{rr} \rangle$  at  $4.57 \cdot 10^{-31} \text{ s}^{-2} \text{ kg}^{-1}$  or  $4.57 \cdot 10^{-19} \text{ mE kg}^{-1}$ . More precisely, if the error affecting the volume of the mass element will cause an error of 1 kg on the mass, then the resulting error on the radial gravity gradient is at  $4.57 \cdot 10^{-19} \text{ mE}$ . As a result, this error reaches 1 mE as the error affecting the mass of source is greater than  $2.19 \cdot 10^{18} \text{ kg}$ .

Now considering the whole Earth's shape as ellipsoidal, the use of the spherical prism as mass element in the numerical calculation of volume integrals such as (7)–(9) gives rise to an error on the resulting effect, which unavoidably increases when the volume of material involved increases. The cumulative error, which affects numerical evaluation of the Earth's mass, can be rigorously calculated using PREM (Dziewonski & Anderson 1981) as follows: the exact value of mass of each Earth's layers defined to be of constant density by PREM, is obtained by summing the mass of each ellipsoidal prism. This value can also be calculated by summing the mass of each corresponding spherical prism. By cumulating the differences between the mass values, cumulative error on mass estimation can be obtained as a function of the layer depth from the Earth's surface. The cumulative error on mass layer estimation has then been transformed into cumulative error on radial gravity gradient  $T_{rr}$  multiplying it by the value of  $\langle \tau_{rr} \rangle$  previously determined.

The cumulative error has been plotted as a function of depth in the graphs shown in Fig. 8 (graph a). As is made clear by the graph,

the error, which affects the numerical calculation of radial gravity gradient, attains 1 mE at 230 km depth and reaches 20 mE when considering the entire radial mass distribution. This confirms that the improper mass estimation, induced by the approximation of the ellipsoidal prism by its spherical counterpart, has a significant effect on the gravity gradient values.

Fortunately, the improper estimation of mass can be easily corrected by scaling the density of each spherical prism. In this case, the scaling factor is simply obtained by calculating the ratio between the volume of the considered ellipsoidal prism and the corresponding spherical prism:

$$\frac{\Omega_{\text{ellip}}}{\Omega_{\text{sph}}} \quad (52)$$

using

$$\Omega_{\text{ellip}} = a^3 (1 - e^2) [\lambda]_{\lambda_1}^{\lambda_2} \left[ \frac{u^3}{3} \right]_{u_1}^{u_2} \left[ \frac{\sin \varphi}{\sqrt{1 - e^2 \sin^2 \varphi}} \right]_{\varphi_1}^{\varphi_2} \quad (53)$$

and

$$\Omega_{\text{sph}} = [\lambda]_{\lambda_1}^{\lambda_2} \left[ \frac{r^3}{3} \right]_{r_1}^{r_2} [\sin \theta]_{\theta_1}^{\theta_2}. \quad (54)$$

By doing so, we do not change the geometrical boundaries given by the geological model. However, there is still an error due to the fact that the Legendre's nodes used in the GLQ involving spherical prisms are slightly different from those involving ellipsoidal prisms. To quantify this remaining error, the previous experiment has been modified as follows: we applied the density scaling correction to eliminate the mass error and we directly calculated the  $T_{rr}$  component, by mean of GLQ, for each layer of PREM at a single point defined by ( $\lambda = 0^\circ, \theta = 50^\circ$  and  $r = 6637655.2$  m, mean radius of GOCE grids). The graph plotted in Fig. 8 (graph b) shows the cumulative difference between the two magnitude values of  $T_{rr}$  gravity gradient, provided, respectively, by the spherical-and ellipsoidal-prism-based methods as a function of depth. This graph shows that the improper location of Legendre's nodes has a smaller effect than the improper mass estimation effect previously established. The error only reaches 1 mE at 830 km depth and 6 mE at the Earth's centre, which suggests that the spherical prism correctly approximates its ellipsoidal counterpart for global lithospheric studies, provided that the scaling of prism densities has been performed. The stabilization of the cumulative error observed for the great depths, is naturally due to the increasing distance between the calculation point and the mass sources coupling with the decrease of the masses involved, thus causing an attenuation of their gravitational effects.

Because of the axial symmetry of the geological model adopted in this experiment, the numerical errors might have offset each other. In order to raise this uncertainty, we experimented on the previous numerical test with a geological model including lateral density changes.

## 4.2 Effect of lateral density changes

In this case, we consider the model of the Earth's interior consisting of the combination of LITHO1.0 model (Pasyanos *et al.* 2014) and PREM model (Dziewonski & Anderson 1981). The former extends from the Earth's surface including topography, ice and water, down to the lithosphere–asthenosphere boundary. It provides, among other physical parameters, the rock densities along column materials of various thicknesses the horizontal size of which is  $1^\circ$  by  $1^\circ$ . The

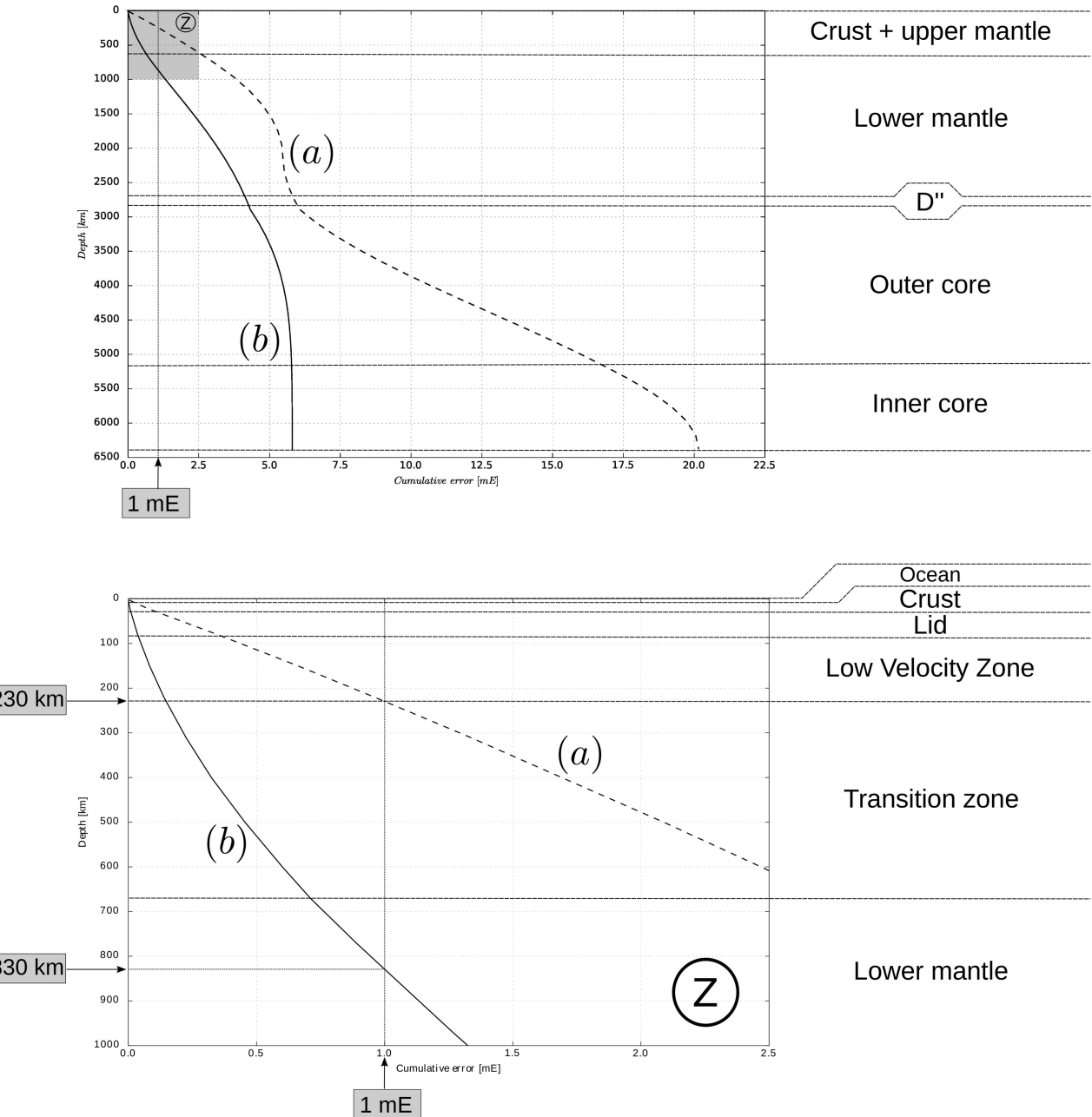


**Figure 8.** (a) Cumulative error on the magnitude of the gravity gradient along the radial direction  $T_{rr}$  at GOCE altitude for Earth's layers of increasing depths. The density distribution as well as the limits of Earth's layers have been provided by PREM. The graph labeled by Z is a zoom showing the first 1000 km. The error results from a misestimation of the volume of each ellipsoidal shape layers when computed from spherical mass elements. Variations of the radial gravity gradient induced by these volume differences have been calculated using the mean value  $\langle \tau_{rr} \rangle$  of the radial gravity gradient variation per unit mass at  $4.57 \times 10^{-19} \text{ mE kg}^{-1}$  determined in the paper. (b) Direct estimation of the error made on the  $T_{rr}$  component when equating the mass of each ellipsoidal and spherical prism by means of a density scaling.

latter entirely described the density distribution as concentric, axially symmetric layers of constant density from the Earth's surface down to the internal core. The densities provided by PREM have been utilized for completing the density distribution given by LITHO1.0 for the remaining part of the Earth's interior, thus giving what we shall henceforth call the combined model. At this point, we can define the gravity anomaly with respect to PREM at GOCE altitude as consisting, for each gravity gradient, of the difference between the gravity gradient values computed from the combined model and that computed at the same points from PREM. The grav-

ity gradients from the sole PREM model can be readily computed by means of the close analytical formulae giving the gravity gradients of an ellipsoid of constant density. To put it more precisely, the gravity effect of PREM can be obtained by adding the respective contributions of concentric and homothetic ellipsoids of constant densities which, once combined, result in the same density distribution as that given by PREM layers. Moreover, the numerical integration by means of GLQ is needed when lateral density variations are present, that is, wherever LITHO1.0 model applies. Since the density distribution given by the combined model beyond 400 km

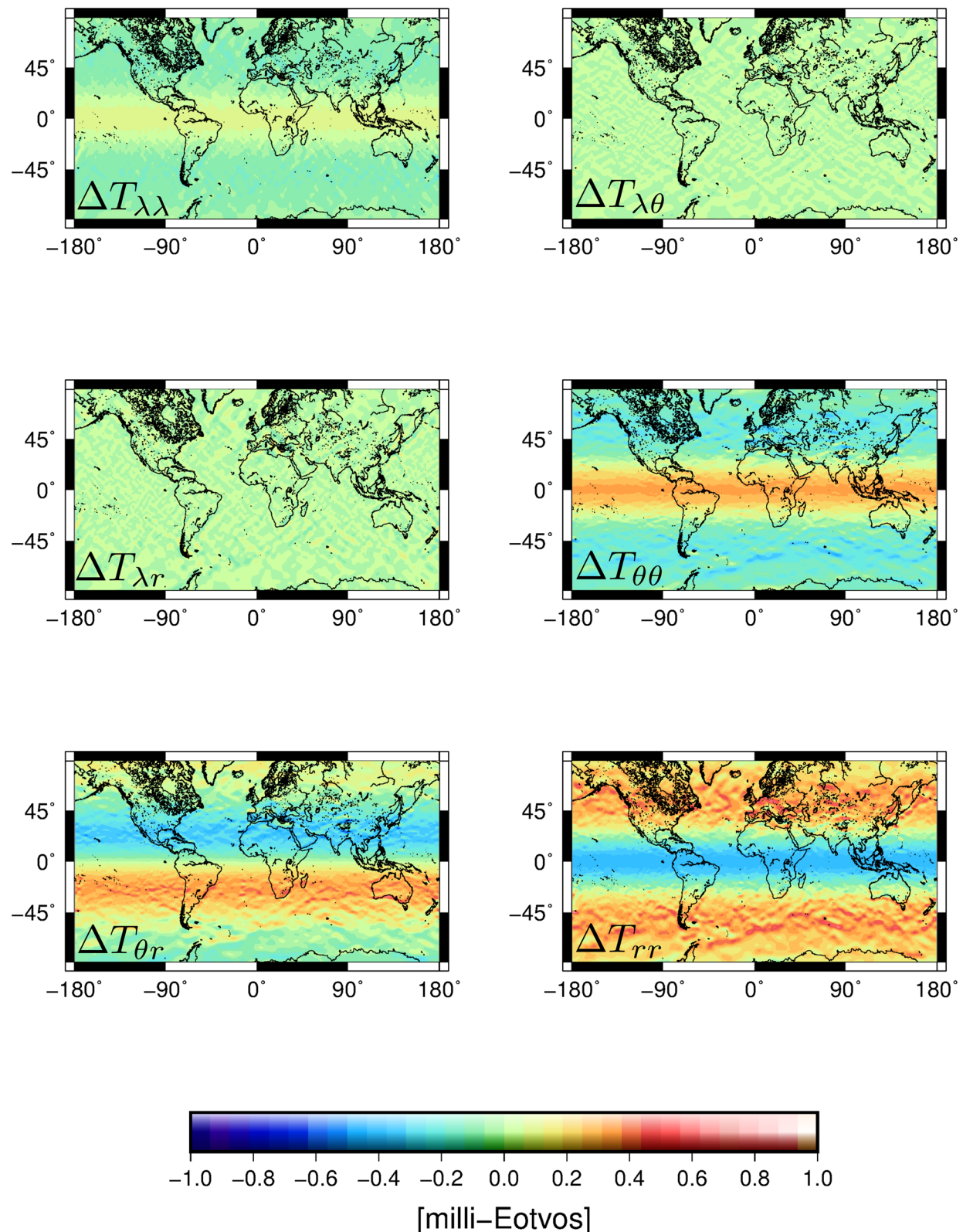


**Figure 9.** Differences between the gravity gradient anomalies produced by the combined model and computed by the two methods (the GLQ using spherical and ellipsoidal prisms).

depth is identical to that of PREM, there is no gravity anomaly with respect to PREM due to the layers located at more than 400 km depth. The gravity gradient anomalies with respect to PREM can therefore be calculated by means of GLQ considering only the first

400 km of the combined model. In that case, the gravity effect to be calculated is that of an ellipsoidal layer of constant thickness with lateral density variations related to the density contrast between LITHO1.0 and PREM distributions.

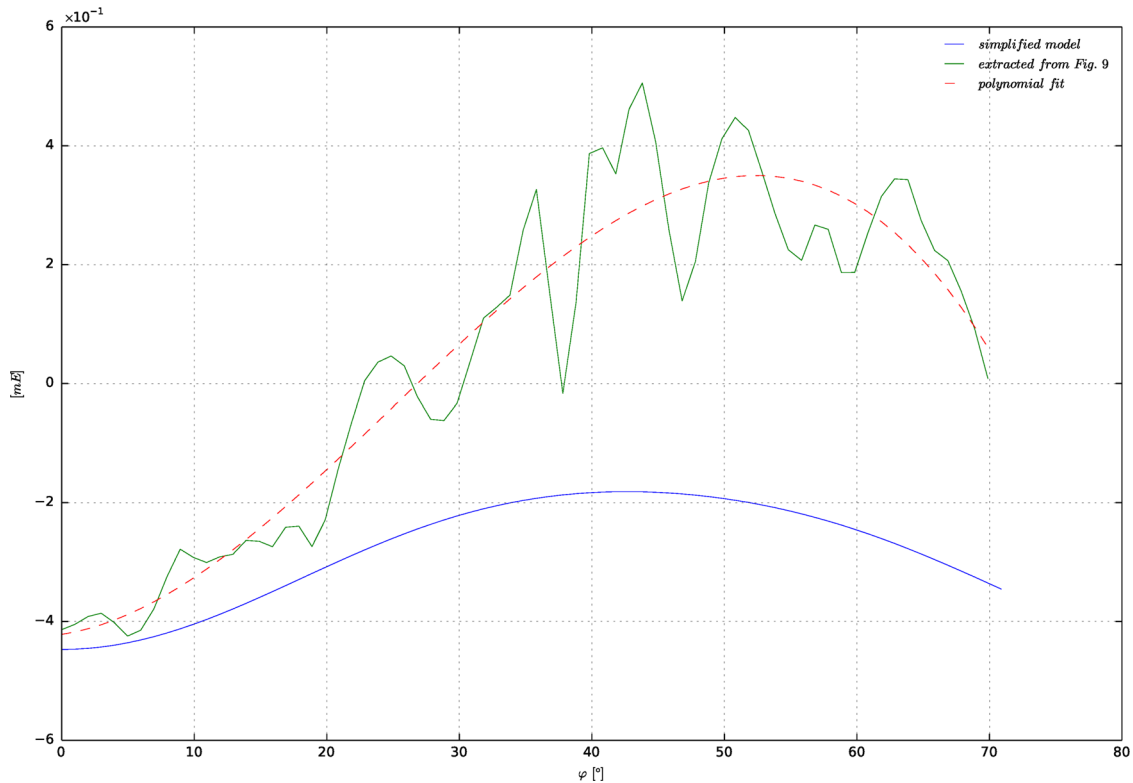


**Figure 10.** The combination of GLQ residual errors relative to the ellipsoidal and spherical prisms (blue plain curve) partly explains the north–south pattern observed on Fig. 9 (green plain and red dashed curves).

Having defined the Earth's model and assuming a perfectly circular orbit of the GOCE satellite, the computation of the resulting gravity gradient anomaly for each gravity gradient over the whole Earth's surface can be carried out by means of GLQ. For the purpose of comparison, these calculations were conducted twice, once using our own method based on ellipsoidal Earth's mass elements, another by means of Tesseroids software (Uieda 2013, op. cit.) based on spherical Earth's mass elements. As in our previous experiment, the mass of each individual spherical prism has been corrected by scaling the density value. The maps of the differences drawn up for six of the nine Marussi's tensor elements on a  $1^\circ \times 1^\circ$  grid, are shown in Fig. 9. Clearly, the magnitude of the approximation error is lesser than 1 mE, which is consistent with results obtained in the previous experiment (Fig. 8, graph b). This finding indicates that lateral density variations do not significantly influence the approximation error. The north–south variations in the differences visible on the maps, particularly for  $T_{\lambda\lambda}$ ,  $T_{\theta\theta}$ ,  $T_{\theta r}$  and  $T_{rr}$ , are likely due to the combination of GLQ residual errors. Indeed, the GLQ residual error for the ellipsoidal prism depends on the adopted quadrature order and varies according to the latitude of the calculation point (Fig. 5). Since similar variations also appear when dealing with the spherical prism, their linear combination may induce patterns such as those illustrated on Fig. 9. This is exemplified by the graph in Fig. 10. The green plain curve corresponds to a north–south profile of the  $T_{rr}$  approximation error that appears in Fig. 9, measured along the meridian of  $0^\circ$  longitude. The error fluctuates along the meridian from the equator to the pole. The overall trend, derived from a polynomial fit (red dashed curve in Fig. 10), shows a peak-to-peak variation of about 0.8 mE from the equator to the poles. To test whether such trend might be attributed to the GLQ, we carried out an experiment consisting in comparing the sole GLQ errors, respectively, from an ellipsoidal and a spherical-prism-based

method. Let  $\epsilon_{\text{ellip}}$  be the GLQ error relative to the ellipsoidal prism. This error has already been determined in Section 3 by using an ellipsoidal shell of constant density whose true gravity effect can be analytically performed (Fig. 5). In the same way, let  $\epsilon_{\text{sph}}$  be the GLQ error relative to spherical prism. This error can be determined by calculating the effect of a spherical shell of constant density. In this particular case, true analytical formulae exist and are directly comparable to those provided by the GLQ. The blue plain curve in Fig. 10 corresponds to the difference between these two residual numerical errors:  $\epsilon_{\text{ellip}} - \epsilon_{\text{sph}}$ . Even if its magnitude does not fit with the red dashed curve (approximation error observed in Fig. 5), it shows the same overall trend, which tends to confirm that the north–south patterns are due to the combination of GLQ residual errors.

## 5 CONCLUSIONS AND OUTLOOK

In this paper, we have been interested in the mathematical formulation of a computational method for calculating by GLQ integration the complete gravity field (gravity potential and vector components and gravity gradients) produced by the Earth's material given a density distribution model. While current integration methods assume a decomposition of the Earth's body into spherical mass elements, our own is essentially based on ellipsoidal mass elements, thus giving an exact decomposition of an ellipsoidally shaped Earth. Because the Marussi's tensor calculated from our method is deliberately expressed in a local spherical basis, the resulting gravity gradients are easily comparable to those measured by GOCE. We have demonstrated by means of simulation using synthetic gravity sources that the error induced by the numerical integration involved in our method is negligible regarding GOCE measurement accuracy

(1 mE). The use of spherical prisms as the mass element for decomposing an ellipsoidal shaped Earth leads to errors on gravity gradient estimates that accumulate when the maximum depth of the Earth's materials involved in the calculation increases. The level reached by the resulting error (<1 mE), such as shown with the combined model involving PREM and LITHO1.0, has proved that the use of the tesseroid is largely suitable for a joint analysis with GOCE data from lithospheric scale, provided that a scaling of prism densities is performed. Alongside a direct comparison between the gravity gradients measured by GOCE and those computed from geophysical Earth's models for the purpose of validation, our method allows us to refine the density distribution models derived solely from terrestrial geophysical methods, by adding satellite gravity data. Indeed, the same mathematical formulation can be used in the inverse problem consisting of determining the Earth's density distribution from gravity measurements, among others. Owing to the fact that ellipsoidal mass elements are intrinsically involved in the calculation of integrals, the method is particularly well suited to ellipsoidal shaped Earth's models.

## ACKNOWLEDGEMENTS

We cordially thank Dimitris Tsoulis, Bert Vermeersen (Editor) and an anonymous reviewer for their comments and suggestions, which significantly contributed to improving the quality of this paper. Fig. 9 was drafted using GMT software (Wessel & Smith 1991). The research was supported by a DGA-MRIS and Pays de la Loire region scholarship. We are also indebted to the French Research Group in Space Geodesy (GRGS) and the CNES (French Space Agency) for its financial support.

## REFERENCES

- Amante, C. & Eakins, B.W., 2009. ETOPO1 1 arc-minute global relief model: procedures, data sources and analysis, Tech. Rep., NOAA Technical Memorandum NESDIS NGDC-24, 19 pp.
- Arabelos, D. & Tsoulis, D., 2013. The exploitation of state of the art digital terrain databases and combined or satellite-only earth gravity models for the estimation of the crust-mantle interface over oceanic regions, *Geophys. J. Int.*, **193**(3), 1343–1352.
- Asgharzadeh, M.F., von Frese, R.R.B., Kim, H.R., Leftwich, T.E. & Kim, J.W., 2007. Spherical prism gravity effects by Gauss-Legendre quadrature integration, *Geophys. J. Int.*, **169**, 1–11.
- Bouman, J. & Fuchs, M.J., 2012. GOCE gravity gradients versus global gravity field models, *Geophys. J. Int.*, **189**, 846–850.
- Bouman, J., Ebbing, J. & Fuchs, M., 2013. Reference frame transformation of satellite gravity gradients and topographic mass reduction, *J. geophys. Res.*, **118**, 759–774.
- Bouman, J. *et al.*, 2015. GOCE gravity gradient data for lithospheric modeling, *Int. J. Appl. Earth Obs. Geoinformation*, **35A**, 16–30.
- Brockmann, J.M., Zehntner, N., Höck, E., Pail, R., Loth, I., Mayer-Gürr, T. & Schuh, W.-D., 2014. EGM\_TIM\_RL05: an independent geoid with centimeter accuracy purely based on the GOCE mission, *Geophys. Res. Lett.*, **41**(22), 8089–8099.
- Bruinsma, S.L., Förste, C., Abrikosov, O., Marty, J.C., Rio, M.-H., Mulet, S. & Bonvalot, S., 2013. The new ESA satellite-only gravity field model via the direct approach, *Geophys. Res. Lett.*, **40**, 3607–3612.
- Cochran, J.R. & Talwani, M., 1978. Gravity anomaly, regional elevation and the deep structure of the North Atlantic, *J. geophys. Res.*, **83**, 4907–4924.
- Dziewonski, A.M. & Anderson, D.L., 1981. Preliminary reference earth model (PREM), *Phys. Earth planet. Inter.*, **25**, 297–356.
- Förste, C. *et al.*, 2014. EIGEN-6C4 the latest combined global gravity field model including GOCE data up to degree and order 2190 of GFZ Potsdam and GRGS Toulouse, in *5th GOCE User Workshop, Paris*, 25–28 November.
- Grombein, T., Seitz, K. & Heck, B., 2013. Optimized formulas for the gravitational field of a tesseroid, *J. Geod.*, **87**(7), 645–660.
- Gruber, T., Rummel, R., Abrikosov, O. & van Hees, R., 2014. *GOCE Level 2 Product Data Handbook (GO-MA-HPF-GS-0110)*, 5th edn, The European GOCE Gravity Consortium (EGG-C).
- Heck, B. & Seitz, K., 2007. A comparison of the tesseroid, prism and point-mass approaches for mass reductions in gravity field modelling, *J. Geod.*, **81**, 121–136.
- Johnson, L.R. & Litehiser, J.J., 1972. A method for computing the gravitational attraction of three-dimensional bodies in a spherical or ellipsoidal Earth, *J. geophys. Res.*, **83**, 6999–7009.
- Kellogg, O.D., 1954. *Foundations of Potential Theory*, Dover Publications, New York, USA.
- Ku, C.C., 1977. A direct computation of gravity and magnetic anomalies caused by 2- and 3-dimensional bodies of arbitrary shape and arbitrary magnetic polarization by equivalent point method and a simplified cubic spline, *Geophysics*, **42**, 610–622.
- Laske, G., Masters, G., Ma, Z. & Pasynko, M., 2013. Update on CRUST1.0 – a 1-degree global model of Earth's crust, in *Research Abstracts, 15, Abstract EGU2013-2658*, 2013.
- MacMillan, W.D., 1930. *Theoretical Mechanics, Vol 2: The Theory of the Potential*, Dover Publications, New York, USA.
- Mooney, W.D., 1998. CRUST 5.1: a global crustal model at  $5^\circ \times 5^\circ$ , *J. geophys. Res.*, **103**, 727–747.
- Nagy, D., 1966. The gravitational attraction of a right rectangular prism, *Geophysics*, **31**, 362–371.
- Nagy, D., Papp, G. & Benedek, J., 2000. The gravitational potential and its derivatives for the prism, *J. Geod.*, **74**, 552–560.
- Panet, I., Pajot-Métivier, G., Greff-Lefftz, M., Métivier, L., Diament, M. & Mandea, M., 2014. Mapping the mass distribution of earth's mantle using satellite-derived gravity gradients, *Nature geosci.*, doi:10.1038/ngeo2063.
- Pasyanos, M.E., Masters, T.G., Laske, G. & Ma, Z., 2014. LITHO1.0: an updated crust and lithospheric model of the Earth, *J. geophys. Res. Solid Earth*, **119**, 2153–2173.
- Paul, M.K., 1974. The gravitational effect of a homogeneous polyhedron for three-dimensional interpretation, *Pure appl. Geophys.*, **112**, 553–561.
- Pavlis, N.K., Holmes, S.A., Kenyon, S.C. & Factor, J.K., 2008. An earth gravitational model to degree 2160: Egm2008, in *Presented at the 2008 General Assembly of the European Geosciences Union, Vienna, Austria, April 13–18*.
- Petrović, S., 1996. Determination of the potential of homogeneous polyhedral bodies using line integrals, *J. Geod.*, **71**, 44–52.
- Plouff, D., 1976. Gravity and magnetic fields of polygonal prisms and application to magnetic terrain corrections, *Geophysics*, **41**, 727–741.
- Rummel, R., Yi, W. & Stummer, C., 2011. GOCE gravitational gradiometry, *J. Geod.*, **85**(11), 777–790.
- Smith, D.A., Robertson, D.S. & Milbert, D.G., 2001. Gravitational attraction of local masses in spherical coordinates, *J. Geod.*, **74**, 783–795.
- Smith, W.H.F. & Sandwell, D.T., 1997. Global seafloor topography from satellite altimetry and ship depth soundings, *Science*, **277**, 1957–1962.
- Talwani, M. & Ewing, M., 1960. Rapid computation of gravitational attraction of three-dimensional bodies of arbitrary shape, *Geophysics*, **25**, 203–225.
- Tsoulis, D., 2012. Analytical computation of the full gravity tensor of a homogeneous arbitrarily shaped polyhedral source using line integrals, *Geophysics*, **77**(2), F1–F11.
- Tsoulis, D., Wziontek, H. & Petrović, S., 2003. A bilinear approximation of the surface relief in terrain correction computations, *J. Geod.*, **77**, 338–344.
- Tsoulis, D., Jamet, O., Verdun, J. & Gonindard, N., 2009. Recursive algorithms for the computation of the potential harmonic coefficients of a constant density polyhedron, *J. Geod.*, **83**(10), 925–942.
- Uieda, L., 2013. Tesseroids: forward modeling of gravitational fields in spherical coordinates, *Figshare*.

- Uieda, L., Bomfim, E.P., Braatenberg, C. & Molina, E., 2011. Optimal forward calculation method of the Marussi tensor due to a geologic structure at GOCE height, in *Proceedings of the 4th International GOCE User Workshop*. Munich, Germany.
- Visser, P.N.M.A., 2011. A glimpse at the GOCE satellite gravity gradient observations, *Adv. Space Res.*, **47**, 393–401.
- von Frese, R.R.B., Hinze, W.J., Braile, L. & Luca, A.J., 1981a. Spherical-earth gravity and magnetic anomaly modeling by Gauss-Legendre quadrature integration, *J. Geophys.*, **49**, 234–242.
- von Frese, R.R.B., Hinze, W.J. & Braile, L.W., 1981b. Spherical-Earth gravity and magnetic anomaly analysis by equivalent source inversion, *Earth Planet. Sci. Lett.*, **53**, 69–83.
- Wessel, P. & Smith, W.H.F., 1991. Free software helps map and display data, *EOS, Trans. Am. geophys. Un.*, **72**, 445–446.
- Wild-Pfeiffer, F., 2008. A comparison of different mass elements for use in gravity gradiometry, *J. Geod.*, **82**(10), 637–653.
- Yi, W. & Rummel, R., 2013. A comparison of GOCE gravitational models with EGM2008, *J. Geodyn.*, **73**, 14–22.